Modular modelling for the power take-off system of a wave energy converter

Master Thesis

Adrián Fernández Vuelta

First supervisor: prof. dr. Bayu Jayawardhana
Second supervisor: dr. Antonis I. Vakis

Industrial Engineering

Groningen, September 2017

Abstract

The Ocean Grazer is a novel ocean energy collection and storage device that has been proposed by the University of Groningen. Its core technology is a wave energy converter that differs from others by its adaptability and capacity to store energy. This thesis presents a modular modelling for the Ocean Grazer's power take-off (PTO) system based on the port-Hamiltonian (PH) framework, which enables energy-based analysis and control of the system. The project aims to obtain a reduced model of the PTO system in order to speed up the computation of control signals, which are essential for the optimal operation of the device. The model is developed in the MATLAB/Simulink environment.

The first part of this thesis is dedicated to the modelling of a point-absorber (PA) device, which is the main unit of the PTO system. It is based on a new modelling concept introduced in a previous work, consisting on breaking down the PA into a moving water mass, a buoy-piston ensemble and a pumping hydraulic system. The model is translated into PH framework and simulation results are compared with previously developed models. The second part deals with the modelling of an array point-absorber devices. First, a reference model is presented, acquiring good agreement with validated models. Afterwards, it is described the identification of the parameters that define the interconnection between the water elements in the present model.

Acknowledgements

First, I would like to thank prof. dr. B. Jayawardhana for giving me the opportunity of working on the Ocean Grazer project. Secondly, I would like to thank prof. dr. B. Jayawardhana and dr. J.J. Barradas-Berglind, who were most involved in my research. They were always open to discuss and help me when I encountered problems.

I would also like to thank dr. Antonis I. Vakis as the second supervisor of my thesis for the feedback during the meeting sessions and dr. Yanji Wei for the explanations and guidance in the development of the floater blanket model.

Furthermore, I would like to thank all the members of the Ocean Grazer group who helped and supported me during my research. In particular I would like to thank Genís Martí, who provided a source of discussion, guidance and entertainment throughout the research process.

Contents

List of Figures

List of Tables

Chapter 1

Introduction

1.1 Renewable energy

Nowadays, roughly 80% of the world primary energy demand is satisfied by fossil fuels, where oil is the leading energy resource. However, there are some challenges that need to be addressed, such as climate change, increased oil prices, issues of security of supply and world population growth. Hence, much attention has turned to renewable energy sources to fulfill future increasing world energy demand. Wind energy has had considerable proliferation, while other sources such as biomass, solar and tidal have enjoyed slightly less deployment.

The role of renewable energies continues to increase in the generation of electricity, being the contribution to the world electricity production by non-hydroelectric renewables of 6,5% in 2014 (EIA). Figure 1.1 shows that most of the electricity generation based on renewable energy sources is produced by hydraulic and wind energies, but only 0,05% is obtained from ocean energy. Wave energy has great potential and therefore it can contribute significantly to the proportion of renewable energy in the global energy share.

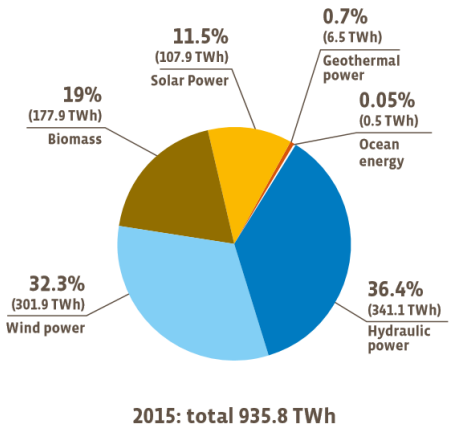

Figure 1.1: Electricity generation by renewable energy in the EU (2015) (Observ'ER, 2016)

The main reason for the lack of proliferation of wave energy is that harnessing the irregular motion of the sea is not as straightforward as, for example, extracting energy from the wind. The relative immaturity of wave-energy technology can be noticed by the existence of just a few commercially available Wave Energy Converters (WECs) as well as by the contrast in their operational principles.

Wave energy can be considered as a concentrated form of solar energy. Winds are generated by the differential heating of earth and, as they pass over open bodies of water, some of their energy is used to create waves. Energy is stored in waves as both potential energy (in the mass of water displaced from the mean sea level) and kinetic energy (in the motion of the water particles).

The global wave power resource in deep water is estimated to be 1-10 TW (Thorpe, 2010). The world distribution of wave energy is depicted in Fig. 1.2, where it can be seen that some countries with high dependence on imported fossil fuels such as Ireland have access to significant wave-energy resources (70 kW/m of wave crest). Furthermore, Ireland has the potential to capture 14 TWh of wave energy per year, which is more than half of its annual energy consumption (Ringwood et al., 2014).

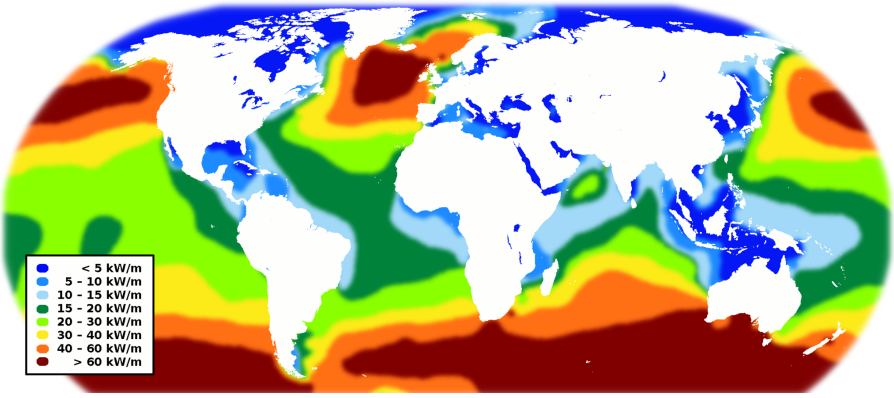

Figure 1.2: World availability of wave energy (Straume, 2014)

Inherent variability in sea conditions (Fig. 1.3) determines the characteristics of the incoming wave, such that each wave may differ significantly from those preceding or following it. Therefore, the WEC should be able to extract energy from both small and large waves for a range of periods.

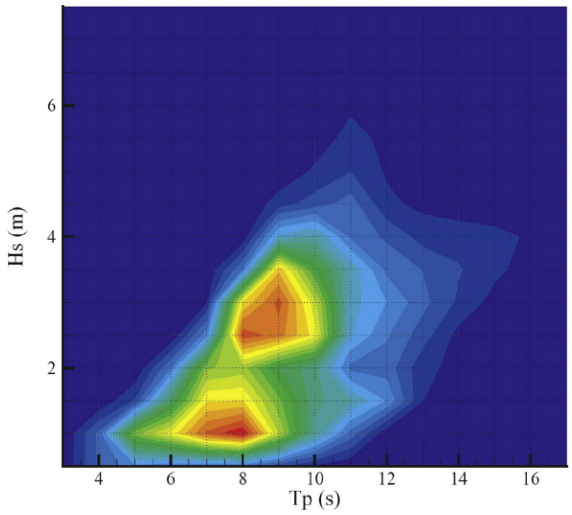

Figure 1.3: Diagram of significant wave heights and characteristic periods for the Atlantic Marine Energy Test Site in Belmullet, Ireland (Ringwood et al., 2014)

1.2 Ocean Grazer

1.2.1 Introduction

The Ocean Grazer is a novel ocean energy collection and storage device that is being developed at the University of Groningen. It is designed to extract and store multiple forms of ocean energy and it consists of several power take-off (PTO) systems, being wave energy the primary source of energy. The device, shown in Fig. 1.4, is a large floating platform located in the ocean more than 50 kilometers off-shore. One single system is expected to produce between 220 to 270 GWh/year, enough energy to fulfill the electricity demand of around 70.000 households. Furthermore, the system will have a loss-free storage capacity of around 800 MWh (Vakis et al., 2014).

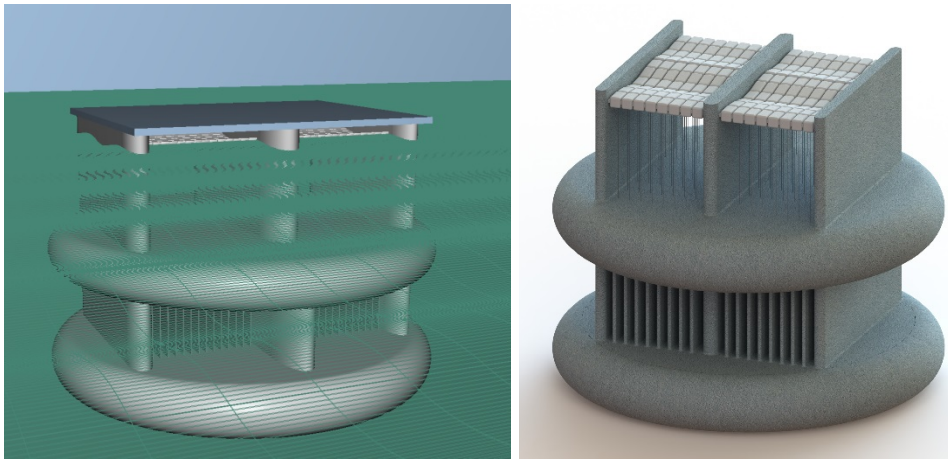

Figure 1.4: The Ocean Grazer submerged (left) and unsubmerged without top platform (right)

The structure is designed to have a diameter of approximately 435 meters and a total height of 255 meters, of which 20 meters above the average seawater level. Under the water surface there would be two reservoirs connected through multiple pumps containing multiple pistons. Its core technology, contributing to about 80% of the energy generation, is a wave energy harvesting device termed the multi-pump multi-piston power take-off (MP^2PTO) system, that differs from other WECs by its adaptability and capacity to store energy.

1.2.2 Multi-pump multi-piston power take-off system

The MP^2PTO, depicted in Fig. 1.5, is based on a point absorber design with the capability to store loss-free potential energy that can be transformed into electricity via a turbine. The system is powered by some interconnected buoys, termed a floater blanket, that follow the motion of the ocean waves and where each floater can be connected to multiple pistons to pump fluid from the lower reservoir to the upper reservoir.

This device has the advantage of decoupling the electricity production from the availability of wave energy. Thus, the upper reservoir acts as an energy buffer that can be used to close the gap between energy supply and demand. The other important feature of the MP^2PTO system is that it is able to adapt itself to maximize the energy extraction for waves ranging in height from 1 to 12 meters and for periods between 4 and 20 seconds. It is claimed to have an average extraction efficiency of about 90% for the aforementioned range (van Rooij, 2015).

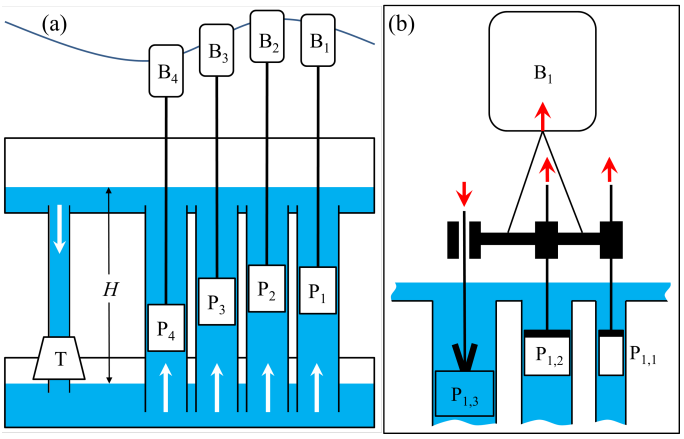

Figure 1.5: Schematic representation of the MP^{2}PTO system

1.3 Goals of the thesis

Previous work has demonstrated the successful potential use of a variable-load control for a multi-piston pump. However, the computation time required can very high, making the deployment in the real device unfeasible. Therefore, it is still a great challenge to develop efficient control strategies for an Ocean Grazer device consisting of hundreds of interconnected floater elements. Control in wave energy applications may rely upon an accurate and high fidelity hydrodynamic model, but working directly with it would increase the complexity and computational cost of the model. Hence, an efficient and accurately enough model is needed.

A time-domain model for ten interconnected floaters has been developed and validated against experimental results and a previous numerical model in (Wei et al., 2017a). The problem that presents this model is that is time consuming: it takes around one day to run 200 seconds of physical time. Recently, in (Wei et al., 2017b), a frequency-domain model with a simple spring-damper PTO system has been proposed, obtaining a considerable reduction of the computation time required.

In (Barradas-Berglind et al., 2016a), it is proposed a first model of one point absorber device based on the port-Hamiltonian (PH) framework, that allows energy-based analysis and control of the system. Furthermore, the modularity that PH framework offers can be useful to interconnect several point-absorber devices in order to model the full MP^{2}PTO system.

Therefore, the main contributions of this thesis can be summarized in:

1. Improvement of the previous port-Hamiltonian model
2. Extension of the model to obtain one-column floater blanket
3. Simulations results and analysis of the system behaviour

The remainder of the thesis is structured as follows. Chapter 2 introduces some theoretical background. In Chapter 3, it is presented the model of a point absorber and simulation results are provided. Subsequently, Chapter 4 describes the model of an array of point-absorber units and the performance of the system is analysed. Finally, conclusions and further work are presented in Chapter 5.

Chapter 2

Theoretical background

In this chapter one can find, firstly, the coordinate system and corresponding nomenclature employed throughout the thesis. Later, it is provided some important information regarding sea waves as well as the theory related with the elements used to develop the model. Lastly, it is introduced the port-Hamiltonian framework, in which we lean on to model the PTO system.

2.1 Coordinate system

Figure 2.1 illustrates a 3D floating point absorber subject to incoming waves propagating in the +X direction. The six degrees of freedom are defined as: surge, sway, heave, roll, pitch and yaw. Surge, sway and heave represent the translation motions along the X, Y and Z axes, respectively. Roll, pitch and yaw are the rotation motions along the X, Y and Z axes, respectively.

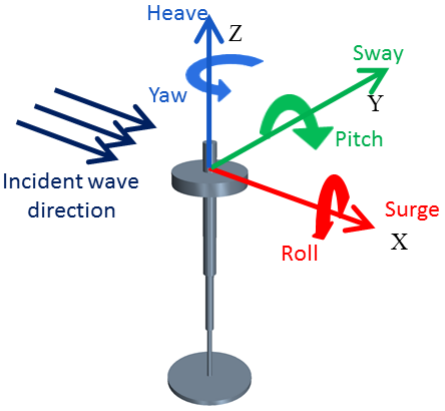

Figure 2.1: Coordinate system (WEC-Sim documentation)

2.2 Sea waves

Sea waves can be generated due to many factors such as wind, an earthquake, astronomical forces or floating structures. Depending on the wavelength, we can distinguish between deep water waves, where the seabed has a negligible effect on the wave, and shallow water waves, if the seabed has a relevant influence on the wave.

Wind waves, especially, are very irregular. Nevertheless, they can be considered as a superposition of simple regular waves, each with its own amplitude ζ_a, wavelength λ, period T and direction of propagation (see Fig. 2.2). The highest point of the wave is the crest and the lowest point is the trough. The amplitude of the wave is the distance from the still water level to the crest and is equal to half of the height, which is the distance between the crest and the trough. The horizontal distance in the direction of wave propagation between any two successive wave crests is the wave length and the distance along the time axis is the wave period.

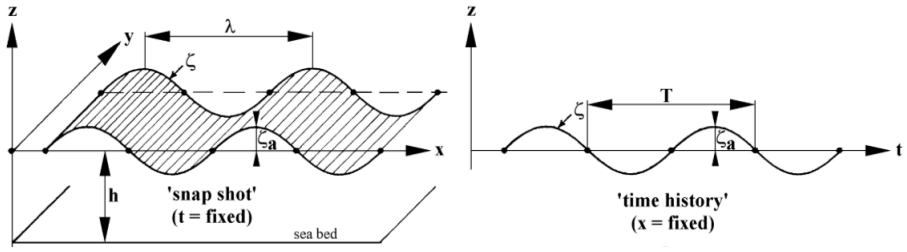

Figure 2.2: Harmonic wave properties (Journée and Massie, 2001)

Thus, each simple wave can be described by

$$\zeta(x,t) = \zeta_a \cos(kx - \omega t) \tag{2.1}$$

with $\zeta(x,t)$ the surface elevation in a certain time t and distance x, $\zeta_a = H/2$ the amplitude, $k = 2\pi/\lambda$ the wave number and $\omega = 2\pi/T$ the frequency. Wave frequency is related to wave number by the dispersion relation

$$\omega^2 = gk \tanh(kh), \tag{2.2}$$

where h is the water depth and g is the acceleration of gravity.

The wave moves one wave length during one period so that its speed or phase velocity c is

$$c = \frac{\lambda}{T}. \tag{2.3}$$

Considering deep water conditions, the particles beneath a wave essentially describe circular orbits, so that their velocities in the $x-$ and $z-$ directions are described by

$$v_x = \zeta_a \omega \cos(kx - \omega t) \tag{2.4a}$$

$$v_z = \zeta_a \omega \sin(kx - \omega t). \tag{2.4b}$$

The average energy content per horizontal area of sea surface as derived from linear wave theory (Falnes, 2002) is given by

$$E = \frac{\rho_{sw} g}{16} H_{m0}^2 \ [\mathrm{J/m^2}], \tag{2.5}$$

where ρ_{sw} is the sea water density and H_{m0} is the significant wave height, which can be replaced by $\sqrt{2}H$ for monochromatic waves, i.e., a sinusoidal wave with a single frequency and phase. The total wave energy is comprised of kinetic and potential energies, contributing each one to half of the total value:

$$E_k = E_p = \frac{\rho_{sw} g}{32} H_{m0}^2 \ [\mathrm{J/m^2}]. \tag{2.6}$$

2.3 Dynamical modelling

In this section, the dynamical models of the basic elements of mechanical and fluid systems are presented. This provides the basis to construct the point absorber system that will be described in Chapter 3.

2.3.1 Mechanical systems

Mechanical systems can be modelled combining three basic ideal elements: masses, springs and dampers.

Masses

Based on Newton's second law, the general equation for an ideal mass m is

$$\sum_{i=1}^{n} F_i = m\frac{d^2x}{dt}, \tag{2.7}$$

where x is the position of the mass and F_i are the applied forces acting upon the mass in the x direction. One mass can be considered as a storage element in terms of kinetic energy if it is moving with a certain velocity

$$E_{k,m} = \frac{1}{2}mv^2, \tag{2.8}$$

and in terms of potential energy depending on the height with respect to a reference position

$$E_{p,m} = mg(h - h_0). \tag{2.9}$$

Springs

An ideal spring (shown in Fig. 2.3), could be defined as a non-mass element that exerts an opposite force as it is stretched or compressed from its rest position, following Hooke's law

$$F_k = k(x - x_0) = k\Delta x, \tag{2.10}$$

where k is the stiffness of the spring, x is the current length of the spring and x_0 is its free length, i.e., the length of the spring when $F_k = 0$. An ideal translational spring stores potential energy as given by

$$E_{p,k} = \frac{1}{2}k\Delta x^2. \tag{2.11}$$

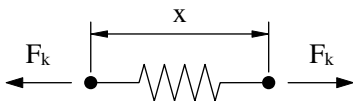

Figure 2.3: Symbolic diagram of a spring

Dampers

Unlike masses and springs, dampers (depicted in Fig. 2.4) do not store energy but dissipate it. The elemental equation for an ideal damper is

$$F_b = b(v_2 - v_1), \tag{2.12}$$

where b is the damping coefficient and $(v_2 - v_1)$ is the relative velocity between its ends. For a damper, the energy dissipated over a time interval is the integral of the instantaneous dissipation power

$$E_{d,b} = \int_{t_1}^{t_2} F_b(v_2 - v_1)\ dt = \int_{t_1}^{t_2} b(v_2 - v_1)^2\ dt. \tag{2.13}$$

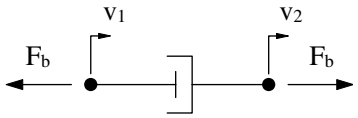

Figure 2.4: Symbolic diagram of a damper

2.3.2 Fluid systems

Fluid systems can be modelled through the following elements: fluid capacitors, fluid inertors, fluid resistors and fluid sources.

Fluid capacitors

Storage tanks and reservoirs work as fluid capacitors (shown in Fig. 2.5) by accumulating the inlet flow, similarly to the process of charging a capacitor in electrical systems.

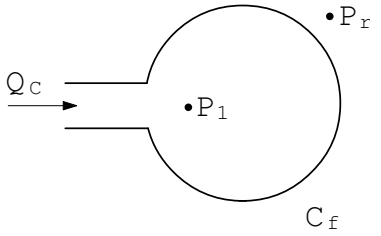

Figure 2.5: Symbolic diagram of a fluid capacitor

The elemental equation for an ideal fluid capacitor is

$$Q_c = C_f \frac{dP_{1r}}{dt}, \tag{2.14}$$

where Q_c is the volume rate of flow into the capacitor, C_f is the fluid capacitance and P_{1r} is the fluid pressure in the capacitor referred to a reference pressure P_r. For an open reservoir, the capacitance is defined by

$$C_f = \frac{A}{\rho g}, \tag{2.15}$$

where A is the cross-sectional area and ρ is the fluid density. The energy stored in a capacitor is potential energy and is related to the work required for increasing the pressure of the fluid filling the capacitor

$$E_{p,c} = \frac{C_f}{2} P_{1r}^2. \tag{2.16}$$

Fluid inertors

Fluid inertors (depicted in Fig. 2.6) indicate the required gradient pressure in a line for producing the change of flow rate involved.

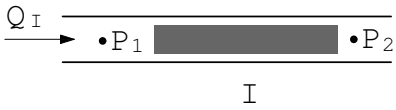

Figure 2.6: Symbolic diagram of a fluid inertor

The elemental equation for an inertor is

$$P_{12} = I \frac{dQ_I}{dt}, \tag{2.17}$$

where P_{12} is the pressure difference between points 1 and 2, I is called the fluid inertance and Q_I is the volume flow rate. For frictionless incompressible flow in an uniform conduct, the inertance I is defined by

$$I = \frac{\rho L}{A}, \tag{2.18}$$

where ρ is the mass density of the fluid, A is the cross-sectional area of the pipe and L is the length of the passage. Inertors store kinetic energy due to the movement of the fluid inside the duct:

$$E_{k,I} = \frac{1}{2} I {Q_I}^2. \tag{2.19}$$

Fluid resistors

Fluid resistance appears in small conducts and usually is consequence of fluid viscosity, which impedes the flow and requires significant pressure gradients. The symbolic diagram of a fluid resistor is shown in Figure 2.7.

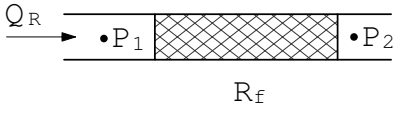

Figure 2.7: Symbolic diagram of a fluid resistor

The elemental equation of an ideal fluid resistor is

$$P_{12} = R_f Q_R, \tag{2.20}$$

where P_{12} is the pressure drop in the resistor, R_f is the fluid resistance and Q_R is the flow rate. A fluid resistor dissipates energy as given by

$$\frac{dE_{d,R}}{dt} = R_f Q_R^2. \tag{2.21}$$

Fluid sources

The input elements in a fluid system are shown Fig. 2.8. An ideal pressure source is able to deliver the indicated pressure, regardless of the flow rate required, whereas an ideal flow source delivers the indicated flow rate, independent of the pressure required.

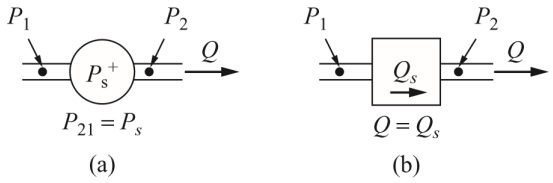

Figure 2.8: Ideal fluid sources: (a) pressure source and (b) flow source (Kulakowski et al., 2007)

2.4 The port-Hamiltonian framework

The port-Hamiltonian (PH) framework is based on the description of a system in terms of energy variables, their interconnection structure and power ports. In fact, the framework of port-based modelling and port-Hamiltonian systems emerges as a general theory for the modelling of complex physical systems from many areas of engineering. Moreover, because of its emphasis on energy and power as the common communication language, PH theory allows the combination of systems from different physical domains (mechanical, electro-magnetic, hydraulic, etc.). Additionally, apart from offering a systematic framework for modelling and analysis of multi-physics systems, it also provides a natural starting point for control, especially in the non-linear case, as the storage function can be used as Lyapunov function.

In general, in port-based modelling, a physical system is described by the interconnection of three types of ideal components: energy-storing elements (inductors, capacitors, masses or springs), energy-dissipating elements (resistors or dampers) and energy-routing elements (transformers, gyrators or ideal constraints) (van der Schaft and Jeltsema, 2014). The energy-storing elements and the energy-dissipating elements are linked to a central interconnection (energy-routing) structure. This linking is done through pairs of equally dimensioned vectors of flow (f) and effort (e) variables; a pair (f,e) of vectors of flow and effort variables is called a port. Figure 2.9 shows three ports: the port (f_S,e_S) linking to an energy storage element, the port (f_R,e_R) corresponding to an energy-dissipation element and the external port (f_P,e_P), by which the system interacts with its environment (including controller action).

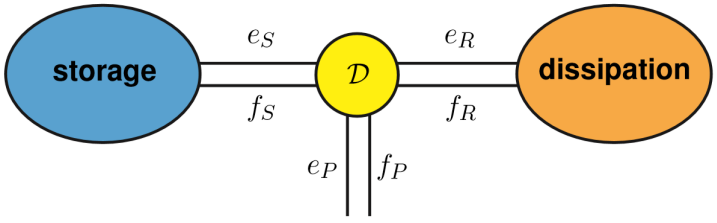

Figure 2.9: Port-Hamiltonian system (van der Schaft and Jeltsema, 2014)

An important particular case of port-Hamiltonian system is the class of *input-state-output port-Hamiltonian system*, which is described by

$$\Sigma = \begin{cases} \dot{x} = [J(x) - R(x)] \frac{\partial H(x)}{\partial x} + g(x)u \\ y = g(x)^\top \frac{\partial H(x)}{\partial x} \end{cases} \tag{2.22}$$

with states $x \in \mathbb{R}^N$, skew-symmetric matrix $J(x) \in \mathbb{R}^{N\times N}$, positive semi-definite matrix $R(x) \in \mathbb{R}^{N\times N}$ that specifies the resistive structure and Hamiltonian $H(x) \in \mathbb{R}$ representing the total energy of the system. The matrix $g(x) \in \mathbb{R}^{N\times M}$ weights the action of the control inputs $u \in \mathbb{R}^M$ on the system and $y \in \mathbb{R}^M$ is output of the system, with $M \leq N$; the pair $(u,\ y)$ form a power port.

For example, a class of mechanical systems wih n degrees of freedom ($N = 2n$) can be described as

$$\Sigma = \begin{cases} \begin{bmatrix} \dot{\varphi} \\ \dot{p}_\varphi \end{bmatrix} = \begin{bmatrix} 0_{n\times n} & I_{n\times n} \\ -I_{n\times n} & -D(\varphi, p_\varphi) \end{bmatrix} \begin{bmatrix} \frac{\partial H(\varphi,p_\varphi)}{\partial \varphi} \\ \frac{\partial H(\varphi,p_\varphi)}{\partial p_\varphi} \end{bmatrix} + \begin{bmatrix} 0_{n\times n} \\ G(\varphi) \end{bmatrix} u \\ y = G(\varphi)^\top \frac{\partial H(\varphi,p_\varphi)}{\partial p_\varphi}, \end{cases} \tag{2.23}$$

with generalized configuration coordinates $\varphi \in \mathbb{R}^n$, generalized momenta $p_\varphi \in \mathbb{R}^n$, damping matrix $D(\varphi, p_\varphi) \in \mathbb{R}^{n\times n}$, where $D(\varphi, p_\varphi) = D(\varphi, p_\varphi)^\top \geq 0$, output $y \in \mathbb{R}^m$, input $u \in \mathbb{R}^m$ and the input matrix $G(\varphi) \in \mathbb{R}^{n\times m}$. Accordingly, the corresponding Hamiltonian is

$$H(\varphi, p_\varphi) = \frac{1}{2} {p_\varphi}^\top M(\varphi)^{-1} p_\varphi + V(\varphi), \tag{2.24}$$

being $M(\varphi) = M(\varphi)^\top > 0$ the generalized mass matrix and $V(\varphi)$ the potential energy.

Energy-routing devices may exchange between different types of energy. A transformer is an element linking two scalar bonds with flow and effort variables (f_1,e_1) $\in \mathbb{R}^2$ and (f_2,e_2) $\in \mathbb{R}^2$ by

$$\begin{aligned} f_2 &= \alpha f_1 \\ e_1 &= -\alpha e_2 \end{aligned} \tag{2.25}$$

with α constant, called the transformer ratio. Similarly, a gyrator is given by the relations

$$\begin{aligned} f_2 &= \beta f_1 \\ \beta e_1 &= -e_2. \end{aligned} \tag{2.26}$$

Energy-routing elements are instrumental to achieve meaningful interconnection of systems. This is an important aspect that will be further discussed in Chapter 3 specifically for the interconnection between the mechanical and fluid subsystems of the PA system.

Chapter 3

Point absorber model

This chapter is organized as follows. Section 3.1 presents the model of a point absorber. Subsequently, the point-absorber system in the PH framework is described in Section 3.2. Lastly, simulation results are provided in Section 3.3.

3.1 Model considered

The point absorber can be divided in the following subsystems: a moving water body representing the wave, a mechanical subsystem consisting of a buoy-piston ensemble that interacts with the water body, a hydraulic subsystem that pumps internal fluid from a lower to an upper reservoir and a switching and coupling stage that allows energy transfer from the mechanical to the hydraulic system and prevents backflow from the upper to the lower reservoir.

In this section, first it is presented a one-degree-of-freedom (1 DOF) dynamical model of a prismatic buoy under the excitation of a simple harmonic wave. Secondly, a description of the hydraulic system is provided and finally the coupling stage that interconnects the previous systems is presented.

3.1.1 Floater motion equation

The general motion equation of a single floater follows Newton's second law:

$$m\ddot{q} = \sum F = F_e + F_r + F_{hs} + F_p, \tag{3.1}$$

where m is the mass of the floater, q is the vertical (heave) displacement of the buoy, F_e is the wave excitation force, F_r is the radiation force, F_{hs} is the restoring force and F_p is the pumping force coming from the hydraulic system. The radiation force and the restoring force are defined respectively as

$$F_r = -m_a(\omega)\ddot{q} + b(\omega)\dot{q} \tag{3.2}$$

and

$$F_{hs} = -kq, \tag{3.3}$$

where m_a and b are the frequency-dependent added-mass and damping coefficients, respectively, and k corresponds to the hydrostatic stiffness. The hydrodynamic coefficients required for the model $-m_a$, $b-$ can be numerically obtained from the Boundary Element Method (BEM) open-source solver Nemoh (Wei et al., 2017b) and are only dependent on the fluid density, the dimensions of the floater and the wave frequency.

Hence, Equation (3.1) turns into

$$(m + m_a)\,\ddot{q} + b\dot{q} + kq = F_e + F_p. \tag{3.4}$$

The excitation force F_e applied to the floater can be defined as given in (3.5), which includes pressure, inertial and damping contributions (Barradas-Berglind et al., 2016b).

$$F_e = (m_a\ddot{\eta} + B\dot{\eta} + K\eta)\,e^{-k_w T}, \tag{3.5}$$

where T is the buoy submersion and $k_w = 2\pi/\lambda_w$ is the wave number for a wave length λ_w. Comparing the amplitude of the excitation force calculated from (3.5) with the value obtained from Nemoh for 1 m wave height (Fig. 3.1), it can be seen that the major difference happens for high frequency values. This is due to the fact that diffraction effects become more important for short-period waves.

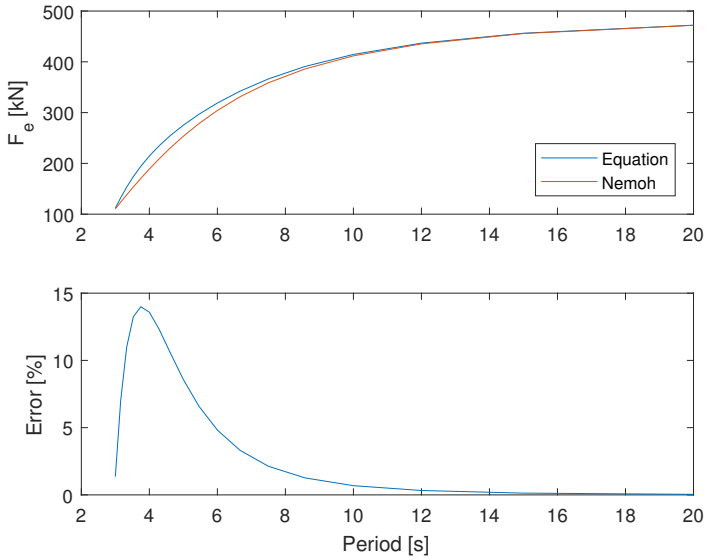

Figure 3.1: Excitation force, F_e

The wave force given in (3.5) can also be expressed in terms of an effective wave elevation as done in (Journée and Massie, 2001):

$$F_e = \left(m_a\ddot{\eta}e^{-k_w T} + B\dot{\eta}e^{-k_w T} + K\eta e^{-k_w T}\right) = \left(m_a\ddot{\eta}^* + B\dot{\eta}^* + K\eta^*\right). \tag{3.6}$$

Considering a constant draft, the excitation force becomes independent of the floater motion, being only function of the wave. In this work, it is assumed that half of the floater is initially submerged in the water.

If having a sinusoidal wave defined as

$$\eta = -\frac{H}{2}\cos(\omega t + \phi) \tag{3.7a}$$

$$\dot{\eta} = \frac{\omega H}{2}\sin(\omega t + \phi) \tag{3.7b}$$

$$\ddot{\eta} = \frac{\omega^2 H}{2}\cos(\omega t + \phi), \tag{3.7c}$$

where H is the wave height and ω the wave frequency, the excitation force given in (3.5) can be expressed as

$$F_e = \frac{H}{2}\left[(m_a\omega^2 - K)\cos(\omega t + \phi) + B\omega\sin(\omega t + \phi)\right]e^{-k_w T}. \tag{3.8}$$

Hence, the amplitude of the excitation force is linear with respect to the wave height H.

Combining (3.4) and (3.6) provides the following equation of motion for the floater

$$(m + m_a)\,\ddot{q} - b\dot{q} - kq = (m_a\ddot{\eta}^* + b\dot{\eta}^* + k\eta^*) + F_p, \tag{3.9}$$

and using the relative motion principle, it can be rewritten as

$$m\ddot{q} = \underbrace{m_a(\ddot{\eta}^* - \ddot{q}) + b(\dot{\eta}^* - \dot{q}) + k(\eta^* - q)}_{Interconnection force} + F_p. \tag{3.10}$$

3.1.2 Moving water body

In order to model the wave-floater interaction in our PA, it is considered a mechanical model of the wave by a simple moving water body described by

$$m_1\ddot{\eta} = F_b + F_w, \tag{3.11}$$

where η is the vertical displacement of the water body, m_1 represents the equivalent mass of the moving water body, F_b corresponds to the forces due to the interaction of the buoy-piston with the moving water mass and F_w is the external force applied to the water body to generate its movement.

Considering deep water conditions, the velocity for heave and surge motions is described by

$$\begin{cases} v_z = \dfrac{\omega H}{2}\sin(\omega t + \phi) & \text{Heave} \\ v_x = -\dfrac{\omega H}{2}\cos(\omega t + \phi) & \text{Surge.} \end{cases} \tag{3.12}$$

Introducing these expressions into the mechanical equation of kinetic energy yields

$$E_k = \frac{1}{2}m_1({v_x}^2 + {v_z}^2) = \frac{1}{8}m_1\omega^2 H^2 \tag{3.13}$$

and taking into account that kinetic energy is half of the total energy water content

$$E_k = \frac{A_w}{16}\rho_{sw} g H^2 \tag{3.14}$$

leads to the following expression for the mass of the water body

$$m_1 = \frac{A_w \rho_{sw} g}{2\omega^2}. \tag{3.15}$$

Note that is dependent on wave frequency, as shown in Fig. 3.2 for a water area $A_w = 49$ m^2 and sea water density $\rho_{sw} = 1025$ kg/m^3.

3.1.3 Buoy-piston ensemble

For simplicity, it is assumed a rigid connection between the buoy and the piston, meaning that they are treated as a single body mass. The dynamics of the buoy-piston ensemble are given by

$$m_2\ddot{q} = -F_b + F_p, \tag{3.16}$$

where q is the displacement of the buoy-piston mass relative to the equilibrium position, m_2 is the equivalent buoy-piston mass, F_b corresponds to the interaction force with the wave and F_p is the

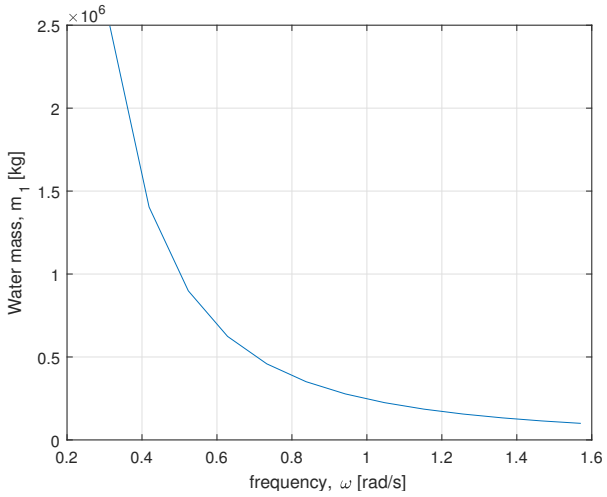

Figure 3.2: Water mass, m_1

pumping force coming from the hydraulic system. In the present work, for the simulation of the mechanical subsystem a simple PTO is considered, consisting on a linear spring-damper system, as shown in (3.17)[1]. The description of the hydraulic F_p will be given in the next section.

$$F_p = -k_{PTO} \cdot q - d_{PTO} \cdot \dot{q}, \tag{3.17}$$

where k_{PTO} and d_{PTO} are the stiffness and damping of the PTO, respectively.

In order to model F_b, a first approach considered is to assume it is simply proportional to the relative displacement and relative velocity between m_1 and m_2:

$$F_b = -k'(\eta - q) - d'(\dot{\eta} - \dot{q}), \tag{3.18}$$

where k' and d' are constant parameters. The schematics of the described system are depicted in Fig. 3.3.

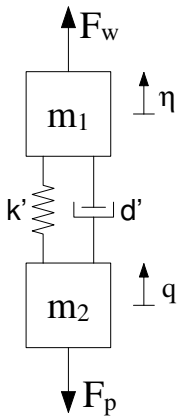

Figure 3.3: Spring-damper connection

These parameters k' and d' have to be obtained. The method used is Least Squares Estimation, as presented in the following.

[1] In the OG-WEC, the pumping force presents a switching behaviour as described in Section 3.1.5.

Introducing (3.17) and (3.18) in (3.16) gives

$$m_2\ddot{q} = k'(\eta - q) + d'(\dot{\eta} - \dot{q}) - k_{PTO} \cdot q - d_{PTO} \cdot \dot{q}$$

and introducing a new variable v defined as

$$v = \dot{q}$$
$$\dot{v} = \ddot{q},$$

Equation (3.16) becomes

$$m_2\dot{v} = k'(\eta - q) + d'(\dot{\eta} - v) - k_{PTO} \cdot q - d_{PTO} \cdot v.$$

Aplying an Euler discretization to the previous expression makes it possible to write

$$\dot{v} \approx \frac{v_{k+1} - v_k}{T_s}$$

$$m_2\frac{v_{k+1} - v_k}{T_s} + k_{PTO} \cdot q_k + d_{PTO} \cdot v_k = k'(\eta_k - q_k) + d'(\dot{\eta}_k - v_k)$$

$$\underbrace{\left[m_2\frac{v_{k+1} - v_k}{T_s} + k_{PTO} \cdot q_k + d_{PTO} \cdot v_k\right]}_{Y} = \underbrace{\begin{bmatrix} \eta_k - q_k & \dot{\eta}_k - v_k \end{bmatrix}}_{\Phi} \cdot \underbrace{\begin{bmatrix} k' \\ d' \end{bmatrix}}_{\theta}$$

$$Y = \Phi \cdot \theta$$

The best estimation of the parameters can be found by

$$\hat{\theta} = (\Phi^\top \Phi)^{-1} \cdot \Phi^\top \cdot Y$$

On the other hand, the same result can be obtained analytically. Assuming η and q to be sinusoidal functions, it can be written

$$\ddot{\eta} = -\omega^2\eta$$
$$\ddot{q} = -\omega^2 q$$

allowing to express the interconnection force in (3.10) as

$$m_a(\ddot{\eta} - \ddot{q}) + b(\dot{\eta} - \dot{q}) + k(\eta - q) = \underbrace{[k - m_a\omega^2]}_{k'} \cdot (\eta - q) + \underbrace{b}_{d'}(\dot{\eta} - \dot{q}) \tag{3.19}$$

obtaining the same parameters k' and d' than with the Least Squares method. Since m_a depends on frequency, k' is also frequency-dependent, as shown in Fig. 3.4.

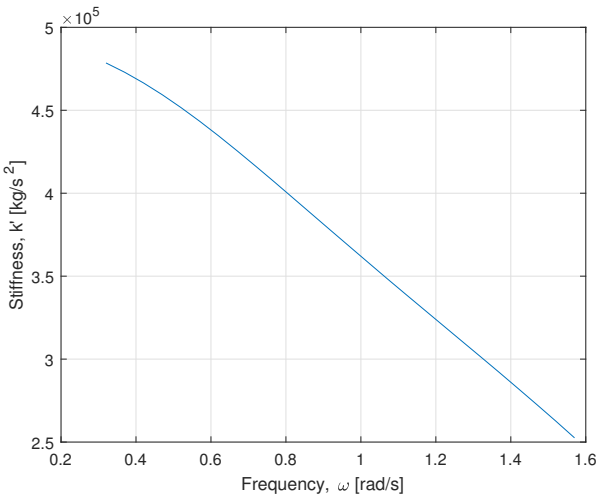

Figure 3.4: Stiffness, k'

Another approach is to introduce a new interconnection element between m_1 and m_2: the inerter (Smith, 2002). The inerter (shown in Fig. 3.5) is defined as *a mechanical two-node (two-terminal), one-port device with the property that the equal and opposite force applied at the nodes is proportional to the relative acceleration between the nodes.* That is

$$F = b(\dot{v}_2 - \dot{v}_1) \tag{3.20}$$

being the constant of proportionality b the intertance with units of kilograms.

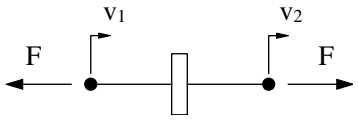

Figure 3.5: Symbolic diagram of an inerter

This new element is presented as the two-terminal device equivalent to the electrical capacitor (see Fig. 3.6).

Mechanical		Electrical	
	$Y(s) = \frac{k}{s}$		$Y(s) = \frac{1}{Ls}$
$\frac{dF}{dt} = k(v_2 - v_1)$	spring	$\frac{di}{dt} = \frac{1}{L}(v_2 - v_1)$	inductor
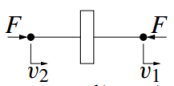	$Y(s) = bs$		$Y(s) = Cs$
$F = b\frac{d(v_2 - v_1)}{dt}$	inerter	$i = C\frac{d(v_2 - v_1)}{dt}$	capacitor
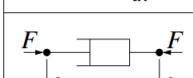	$Y(s) = c$	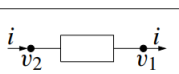	$Y(s) = \frac{1}{R}$
$F = c(v_2 - v_1)$	damper	$i = \frac{1}{R}(v_2 - v_1)$	resistor

Figure 3.6: Circuit symbols and correspondences (Smith, 2002)

The stored energy in the inerter is defined as

$$E = \frac{1}{2}b(v_2 - v_1)^2. \tag{3.21}$$

Including this new element into the connection force leads to Equation (3.22), which is represented in Fig. 3.7.

$$F_b = -k(\eta - q) - d(\dot{\eta} - \dot{q}) - m_a(\ddot{\eta} - \ddot{q}). \tag{3.22}$$

Note that this equation is the same as in (3.10)[2].

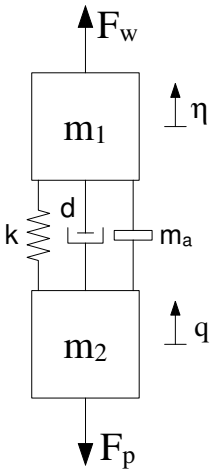

Figure 3.7: Spring-damper-inerter connection

3.1.4 Pumping hydraulic system

Original model

The hydraulic system consists of a lower reservoir and an upper reservoir with cross-sectional areas A_l and A_u, respectively, connected through a pipe with length L_{16}. This connection can be described by two inertors $I_{12}, I_{56} > 0$, two resistors $R_{23}, R_{45} > 0$ and a pressure source $P_{34} = P_s$ (Barradas-Berglind et al., 2016a), as depicted in Figure 3.8.

To satisfy the compatibility law, the pressures in the system are related by

$$P_1 - P_6 = P_{16} = P_{12} + P_{23} + P_s + P_{45} + P_{56} \tag{3.23}$$

which is equivalent to

$$P_s = P_{16} + P_{21} + P_{32} + P_{54} + P_{65}. \tag{3.24}$$

Describing the individual pressures at each component, the pressures in the inertors can be written as

$$P_{21} = \frac{\rho L_{12}}{A_c}\dot{Q} + g\rho L_{12} = I_{12}\dot{Q} + g\rho L_{12} \tag{3.25a}$$

$$P_{65} = \frac{\rho L_{56}}{A_c}\dot{Q} + g\rho L_{56} = I_{56}\dot{Q} + g\rho L_{56} \tag{3.25b}$$

[2]Recall that F_b is negative in (3.16).

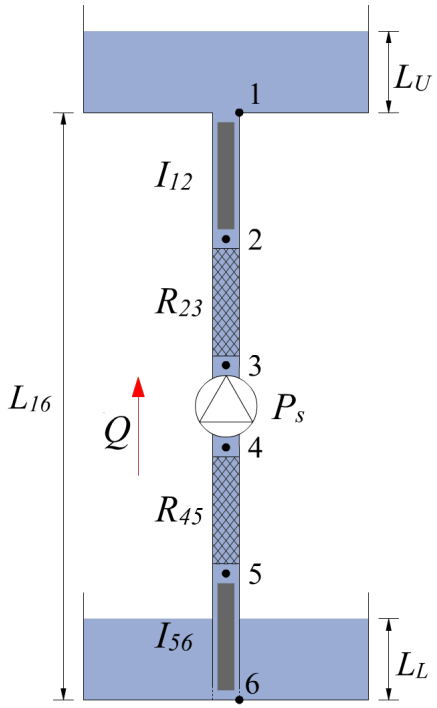

Figure 3.8: Pumping hydraulic subsystem

and the pressures in the resistors are given by

$$P_{32} = \frac{8\mu\pi L_{23}}{A_c^2}Q + g\rho L_{23} = R_{23}Q + g\rho L_{23} \tag{3.26a}$$

$$P_{54} = \frac{8\mu\pi L_{45}}{A_c^2}Q + g\rho L_{45} = R_{45}Q + g\rho L_{45}, \tag{3.26b}$$

with $L_{12}, L_{23}, L_{45}, L_{56}$ being the water column heights of the system. Inserting (3.25) and (3.26) in (3.24) yields

$$I\dot{Q} = -RQ + P_s - P_{16} - \rho g L_{16} \tag{3.27}$$

with the equivalent intertance $I = I_{12} + I_{56}$, the equivalent resistance $R = R_{23} + R_{45}$ and the equivalent water column height $L_{16} = L_{12} + L_{23} + L_{45} + L_{56}$.

Combining the above equations into the pumping force expression gives

$$\begin{aligned} F_p = A_c P_s &= A_c P_{16} + \rho(L_{12} + L_{56})\dot{Q} + g\rho A_c(L_{12} + L_{23} + L_{45} + L_{56}) + \frac{8\mu\pi(L_{23} + L_{45})}{A_c}Q \\ &= A_c P_{16} + \rho\frac{L_{16}}{2}\dot{Q} + g\rho A_c L_{16} + \frac{8\mu\pi}{A_c}\frac{L_{16}}{2}Q = A_c P_{16} + I A_c\dot{Q} + g\rho A_c L_{16} + R A_c Q. \end{aligned} \tag{3.28}$$

Furthermore, the dynamics of P_{16} can be written as the difference between the change in the pressures at the upper and lower reservoirs as

$$\dot{P}_{16} = \frac{\rho g}{A_U}Q - \left(-\frac{\rho g}{A_L}Q\right) = \frac{1}{C_{13}}Q - \left(-\frac{1}{C_{46}}Q\right) \tag{3.29}$$

with the upper reservoir capacitance $1/C_{13}$ and lower reservoir capacitance $1/C_{46}$, or more compactly as

$$C\dot{P}_{16} = Q \tag{3.30}$$

with the equivalent capacitance $C = \frac{C_{13}C_{46}}{C_{13}+C_{46}}$.

Additional terms

Comparing this model with the SPP hydraulic model proposed in (Vakis and Anagnostopoulos, 2016), the latter presents the following major differences:

1. The pressure gradient between points 1 and 2 includes an additional term involving the dynamically varying hydraulic head in the upper reservoir calculated as a function of pressure at point 1, i.e.
$$P_{21} = \frac{\rho(L_{12} + L_u)}{A_c}\dot{Q} + g\rho L_{12}, \qquad L_u = \frac{p_1}{\rho g} \tag{3.31}$$
2. The pressure gradient between points 5 and 6 includes an additional term $\rho\dot{q}^2$, representing the change in momentum needed to accelerate the working fluid that enters the cylinder from the lower reservoir in order to attain the velocity of the moving fluid column.
3. The pressure gradient is described by two inertors, neglecting losses due to the wall friction, instead of the combination of inertor-resistor presented in the previous section.

If including the first two terms described, the expression for the pumping force becomes
$$F_p = A_c P_{16} + IA_c\dot{Q} + \underbrace{\rho L_u \dot{Q}}_{\text{First term}} + g\rho A_c L_{16} + RA_c Q + \underbrace{A_c\rho\dot{q}^2}_{\text{Second term}} \tag{3.32}$$
or equivalently,
$$P_s = P_{16} + \left(I + \frac{\rho L_u}{A_c}\right)\dot{Q} + g\rho L_{16} + RQ + \rho\dot{q}^2,$$
which taking into account that $Q = A_c\dot{q}$, it can be rewritten as
$$P_s = P_{16} + \left(I + \frac{\rho L_u}{A_c}\right)\dot{Q} + g\rho L_{16} + RQ + \frac{\rho Q^2}{Ac^2}. \tag{3.33}$$

3.1.5 Switched buoy-piston-pump system[3]

The use of piston flaps and check valves introduces a switching behaviour in the point-absorber system. When $\dot{q} > 0$ (the piston is moving upward), the pump is activated such that $Q > 0$ and $P_s > 0$. Otherwise, both $Q = 0$ and $P_s = 0$ (the piston is moving downward). This switching mechanism in the pumping system enables to: (i) transfer kinetic energy from the water body into potential energy of the working fluid in the upstroke and (ii) prevent the reverse energy transfer during the downstroke.

Therefore, when the working fluid is allowed to flow, we have the coupling $Q = A_c\dot{q}$ and $F_p = A_c P_s$. Hence, when $\dot{q} > 0$, combining (3.27), (3.30) and (3.16) gives the coupled buoy-piston-pump system
$$(m_2 + IA_c^2)\ddot{q} = -F_b - RA_c^2\dot{q} - A_c P_{16} - g\rho L_{16}A_c \tag{3.34a}$$
$$C\dot{P}_{16} = A_c\dot{q}. \tag{3.34b}$$

On the other hand, when $\dot{q} \leq 0$, we have
$$m_2\ddot{q} = -F_b \tag{3.35a}$$
$$C\dot{P}_{16} = 0 \tag{3.35b}$$

[3]In this section, it is presented the interconnection stage between the mechanical and hydraulic subsystems, therefore here it is not considered the spring-damper PTO force but the real pumping force coming from the hydraulic system.

such that the buoy-piston decouples from the pumping system. Equations (3.34) and (3.35) together with (3.11) define the basic operation of a single PA unit.

Besides, due to the significant hydraulic head difference between the upper reservoir and the lower reservoir, the pumping force can be very large during the upstroke and becomes zero during the downstroke. This instantaneously switching behaviour may introduce discontinuities to the system; to avoid it, it can be used exponential growth and decay terms to calculate the fluid column mass (Vakis and Anagnostopoulos, 2016) or a dynamically varying area of the piston (Wei et al., 2017a).

Therefore, taking into account all the previous systems, the point-absorber device can be described as shown in Fig. 3.9, such that it is a modular element that can be connected to other point absorbers.

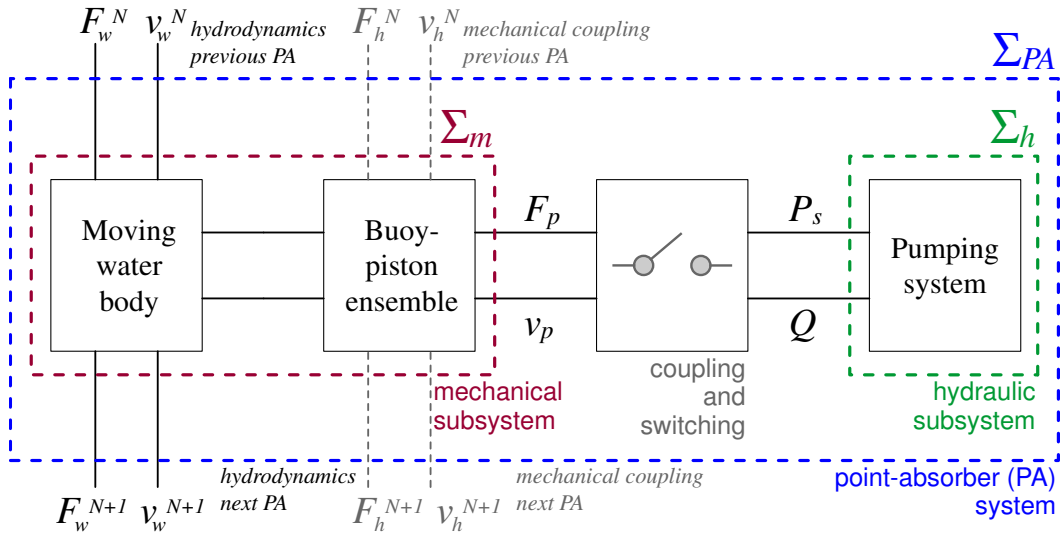

Figure 3.9: Interconnected point-absorber (PA) system Σ_{PA} schematic with its respective subsystems: the mechanical subsystem Σ_m, the hydraulic subsystem Σ_h and the coupling stage between them. Furthermore, the potential connection to other PAs is shown through hydrodynamics and mechanical couplings (Barradas-Berglind et al., 2016a)

3.2 Power take-off system in the PH framework

In this section, it is described the mechanical and hydraulic subsystems (Σ_m and Σ_h respectively) in the PH framework. Afterwards, it is presented the interconnection stage, allowing the transfer of kinetic energy from the mechanical subsystem to the hydraulic subsystem and impeding the reverse energy transfer. Lastly, it is shown the passivity property of the interconnected system and the correct storage of potential energy.

3.2.1 Mechanical subsystem

Spring-damper connection

Consider the water body displacement η in (3.11) and the buoy-piston displacement in (3.16) as the generalized coordinates of the mechanical subsystem. The generalized momenta of the water

mass and the buoy-piston are defined by $p_\eta = m_1\dot{\eta}$ and $p_q = m_2\dot{q}$, respectively. Hence, the state vector is $x_m = [\eta\ q\ p_\eta\ p_q]^\top$, such that the mechanical subsystem can be written as

$$\Sigma_m = \begin{cases} \dot{x}_m = \begin{bmatrix} 0_{2\times2} & I_{2\times2} \\ -I_{2\times2} & -D_m \end{bmatrix} \frac{\partial H_m(x_m)}{\partial x_m} + \begin{bmatrix} 0_{2\times2} \\ I_{2\times2} \end{bmatrix} u_m \\ y_m = \begin{bmatrix} 0_{2\times2} & I_{2\times2} \end{bmatrix} \frac{\partial H_m(x_m)}{\partial x_m}, \end{cases} \tag{3.36}$$

where $0_{2\times2}$ is the null matrix, $I_{2\times2}$ represents the identity matrix, D_m is the dissipation matrix and with the external power port (u_m, y_m) defined as

$$u_m = [u_{m,1}\ u_{m,2}]^\top = [F_w\ F_p]^\top \tag{3.37a}$$

$$y_m = [y_{m,1}\ y_{m,2}]^\top = \left[\frac{1}{m_1}p_\eta\ \frac{1}{m_2}p_q\right]^\top = [\dot{\eta}\ \dot{q}]^\top. \tag{3.37b}$$

The dissipation term is defined by

$$D_m = \begin{bmatrix} d' & -d' \\ -d' & d' \end{bmatrix}, \tag{3.38}$$

with $d' > 0$ being the damping coefficient between masses m_1 and m_2. The system can be described as done in (2.22) by defining the matrices J_m and R_m as

$$J_m = \begin{bmatrix} 0_{2\times2} & I_{2\times2} \\ -I_{2\times2} & 0_{2\times2} \end{bmatrix} \qquad \text{and} \qquad R_m = \begin{bmatrix} 0_{2\times2} & 0_{2\times2} \\ 0_{2\times2} & D_m \end{bmatrix}. \tag{3.39}$$

Note that $J_m = -J_m^\top$ and $R_m \geq 0$ since $D_m \geq 0$. The corresponding Hamiltonian or energy function of the mechanical subsystem Σ_m is the sum of the energies of the storage elements, i.e.

$$H_m(x_m) = \frac{1}{2}\frac{1}{m_1}{p_\eta}^2 + \frac{1}{2}k'(\eta - q)^2 + \frac{1}{2}\frac{1}{m_2}{p_q}^2 \tag{3.40}$$

being m_1 the equivalent water mass body, m_2 the mass of the piston-buoy ensemble and $k' > 0$ the spring stiffness. Note that $H_m(x_m) \geq 0$. This function is comprised of kinetic and potential energies:

$$E_{k,\Sigma_m} = \frac{1}{2}\frac{1}{m_1}{p_\eta}^2 + \frac{1}{2}\frac{1}{m_2}{p_q}^2 = \frac{1}{2}\begin{bmatrix} p_\eta & p_q \end{bmatrix} \cdot \begin{bmatrix} 1/m_1 & 0 \\ 0 & 1/m_2 \end{bmatrix} \cdot \begin{bmatrix} p_\eta \\ p_q \end{bmatrix} = \frac{1}{2}p^\top M^{-1} p \tag{3.41a}$$

$$E_{p,\Sigma_m} = \frac{1}{2}k'(\eta - q)^2 + \frac{1}{2}k_{PTO}q^2 = \frac{1}{2}\begin{bmatrix} \eta & q \end{bmatrix} \cdot \begin{bmatrix} k' & -k' \\ -k' & k' + k_{PTO} \end{bmatrix} \cdot \begin{bmatrix} \eta \\ q \end{bmatrix} = \frac{1}{2}x^\top K x. \tag{3.41b}$$

Spring-damper-inerter connection

Combining the motion equations (3.11) and (3.16) together with the interconnection force given in (3.22), it can be obtained the following expressions:

$$\begin{cases} (m_1m_2 + m_1m_a + m_2m_a)\ddot{\eta} = (m_2 + m_a)\cdot F_w - m_2k(\eta - q) - m_2d(\dot{\eta} - \dot{q}) + m_aF_p \\ (m_1m_2 + m_1m_a + m_2m_a)\ddot{q} = m_aF_w + m_1k(\eta - q) + m_1d(\dot{\eta} - \dot{q}) + (m_1 + m_a)\cdot F_p. \end{cases} \tag{3.42}$$

Defining a new parameter M as

$$M = m_1m_2 + m_1m_a + m_2m_a, \tag{3.43}$$

the mechanical subsystem can be written as

$$\Sigma_m = \begin{cases} \dot{x}_m = \begin{bmatrix} 0_{2\times2} & \xi_{2\times2} \\ -\xi_{2\times2} & -D_m \end{bmatrix} \frac{\partial H_m(x_m)}{\partial x_m} + \begin{bmatrix} 0_{2\times2} \\ {\xi_{2\times2}}^\top \end{bmatrix} \cdot u_m \\ y_m = \begin{bmatrix} 0_{2\times2} & \xi_{2\times2} \end{bmatrix} \frac{\partial H_m(x_m)}{\partial x_m} \end{cases} \tag{3.44}$$

being

$$\xi_{2\times2} = \frac{1}{M} \begin{bmatrix} m_1(m_2+m_a) & m_2 m_a \\ m_1 m_a & m_2(m_1+m_a) \end{bmatrix}, \qquad D_m = \left(\frac{m_1 m_2}{M}\right)^2 \cdot \begin{bmatrix} d & -d \\ -d & d \end{bmatrix}. \tag{3.45}$$

Note that the structure of the system is similar to the previous one while the external port remains the same:

$$u_m = [u_{m,1}\ u_{m,2}]^\top = [F_w\ F_p]^\top \tag{3.46a}$$

$$y_m = [y_{m,1}\ y_{m,2}]^\top = [\dot{\eta}\ \dot{q}]^\top. \tag{3.46b}$$

In this case, the matrices J_m and R_m are

$$J_m = \begin{bmatrix} 0_{2\times2} & \xi_{2\times2} \\ -\xi_{2\times2} & 0_{2\times2} \end{bmatrix} \qquad \text{and} \qquad R_m = \begin{bmatrix} 0_{2\times2} & 0_{2\times2} \\ 0_{2\times2} & D_m \end{bmatrix}. \tag{3.47}$$

Note that $J_m = -J_m^\top$ and $R_m \geq 0$ since $D_m \geq 0$.

The Hamiltonian of the mechanical subsystem Σ_m is

$$H_m(x_m) = \frac{1}{2}\frac{1}{m_1}{p_\eta}^2 + \frac{1}{2}k(\eta - q)^2 + \frac{1}{2}\frac{1}{m_2}{p_q}^2 + \frac{1}{2}m_a\left(\frac{p_\eta}{m_1} - \frac{p_q}{m_2}\right)^2 \tag{3.48}$$

with m_a being the added mass. Note that $H_m(x_m) \geq 0$. Kinetic and potential energies can be written as

$$E_{k,\Sigma_m} = \frac{1}{2}\frac{1}{m_1}{p_\eta}^2 + \frac{1}{2}\frac{1}{m_2}{p_q}^2 + \frac{1}{2}m_a\left(\frac{p_\eta}{m_1} - \frac{p_q}{m_2}\right)^2 \tag{3.49a}$$

$$E_{p,\Sigma_m} = \frac{1}{2}k(\eta - q)^2. \tag{3.49b}$$

3.2.2 Hydraulic subsystem

Original model

Let the state vector of the hydraulic subsystem be composed of the pressure difference between the upper and the lower reservoir and the flow rate of internal fluid: $x_h = \begin{bmatrix} P_{16}\ Q \end{bmatrix}^\top$. Thus, the hydraulic subsystem can be written as

$$\Sigma_h = \begin{cases} \dot{x}_h = \begin{bmatrix} 0 & 1/CI \\ -1/CI & -R/I^2 \end{bmatrix} \frac{\partial H_h(x_h)}{\partial x_h} + \begin{bmatrix} 0 \\ \frac{1}{I} \end{bmatrix} u_h \\ y_h = \begin{bmatrix} 0 & 1/I \end{bmatrix} \frac{\partial H_h(x_h)}{\partial x_h}, \end{cases} \tag{3.50}$$

with an external power port (u_h,y_h) given by

$$u_h = P_s \tag{3.51a}$$
$$y_h = Q. \tag{3.51b}$$

It follows from (3.50) that the interconnection and damping matrices are

$$J_h = \begin{bmatrix} 0 & 1/CI \\ -1/CI & 0 \end{bmatrix} \qquad \text{and} \qquad R_h = \begin{bmatrix} 0 & 0 \\ 0 & R/I^2 \end{bmatrix}. \tag{3.52}$$

It can be verified that $J_h = -J_h^\top$ and $R_h \geq 0$ since $R/I^2 \geq 0$.

The potential energy of the system is given by

$$\begin{aligned} E_{p,\Sigma_h} &= \int P_{potential}\ dt = \int \rho g \overbrace{(L_{16} + L_U - L_L)}^{H} Q\ dt \\ &= \int \rho g \left(L_{16} + \frac{P_{16}}{\rho g} \right) C\dot{P}_{16}\ dt = C\rho g L_{16} P_{16} + \frac{1}{2} C P_{16}^2 + K. \end{aligned} \tag{3.53}$$

Considering the initial potential energy to be zero, the constant K can be determined by

$$K = -C\rho g L_{16} P_{16,0} - \frac{1}{2} C P_{16,0}^2,$$

where $P_{16,0}$ is the initial value of P_{16}. Therefore, it follows that $E_{p,\Sigma_h} \geq 0$ since

$$\begin{cases} \dot{E}_{p,\Sigma_h} = P_{potential} \geq 0 \\ E_{p,\Sigma_h}(t=0) = 0. \end{cases}$$

In addition, the kinetic energy has the following expression

$$E_{k,\Sigma_h} = \frac{1}{2} I Q^2. \tag{3.54}$$

Consequently, the Hamiltonian can be written as

$$H_h(x_h) = \frac{1}{2} C P_{16}^2 + \frac{1}{2} I Q^2 + C g \rho_c L_{16} P_{16} + K. \tag{3.55}$$

Note that $H_h(x_h) \geq 0$.

Additional terms

In the present work, it has been introduced the second term from 3.1.4. The first term involves a dynamically varying variable and further investigation would be needed. Thus, the hydraulic subsystem can be written as

$$\Sigma_h = \begin{cases} \dot{x}_h = \begin{bmatrix} 0 & 1/CI \\ -1/CI & -R/I^2 - \frac{\rho Q}{I^2 A c^2} \end{bmatrix} \frac{\partial H_h(x_h)}{\partial x_h} + \begin{bmatrix} 0 \\ \frac{1}{I} \end{bmatrix} u_h \\ y_h = \begin{bmatrix} 0 & 1/I \end{bmatrix} \frac{\partial H_h(x_h)}{\partial x_h}, \end{cases} \tag{3.56}$$

where the interconnection and damping matrices are

$$J_h = \begin{bmatrix} 0 & 1/CI \\ -1/CI & 0 \end{bmatrix} \text{ and } R_h = \begin{bmatrix} 0 & 0 \\ 0 & R/I^2 + \frac{\rho Q}{I^2 A c^2} \end{bmatrix} \tag{3.57}$$

and with the same external port as in (3.51).

It follows that $J_h = -J_h^\top$ and $R_h \geq 0$ since $R/I^2 + \rho Q/(I^2 A c^2) \geq 0$. In this case, the dissipation term is attributable to the resistor element and the losses due to the transfer of momentum of the moving fluid column to the stationary fluid in the lower reservoir. Now, the dissipation rate is given by

$$\frac{dE_{diss}}{dt} = RQ^2 + \frac{\rho Q^3}{A_c^2}. \tag{3.58}$$

3.2.3 Interconnected system

As discussed in Section 3.1.5, the hydraulic subsystem introduces a switching behaviour between the upward and downward movement[4]. It can be formalized through a binary variable σ defined by

$$\sigma = \begin{cases} 1 & \text{for } \dot{q} \text{ and } F_p > 0 \\ 0 & \text{otherwise} \end{cases} \tag{3.59}$$

such that the hydraulic subsystem becomes

$$\Sigma_h = \begin{cases} \dot{x}_h = (\sigma J_h - \sigma D_h) \frac{\partial H_h(x_h)}{\partial x_h} + \begin{bmatrix} 0 \\ \frac{\sigma^2}{I} \end{bmatrix} P_s \\ y_h = \sigma^2 Q \end{cases} \tag{3.60}$$

while the mechanical subsystem remains the same. Finally, the interconnection can be redefined by using a transformer element (Barradas-Berglind et al., 2016a)

$$u_{m,2} = -\sigma A_c u_h$$
$$\sigma y_h = A_c y_{m,2}$$

or equivalently,

$$F_p = -\sigma A_c P_s \tag{3.62a}$$
$$\sigma Q = A_c \dot{q}. \tag{3.62b}$$

Note that this linkage is not the usual input-output interconnection where the output of one system is connected to the input of the other system.

Hence, for $\sigma = 1$ Σ_m and Σ_h are coupled, whereas $\sigma = 0$ leads to

$$F_p = 0 \tag{3.63a}$$
$$0 = A_c \dot{q} \tag{3.63b}$$

effectively decoupling Σ_h from Σ_m.

Considering the Hamiltonian of the interconnected system as

$$H_{pa}(x_m, x_h) = H_m(x_m) + H_h(x_h), \tag{3.64}$$

it can be checked that the PA system resulting from the interconnection of the mechanical subsystem Σ_m[5] and the hydraulic subsystem Σ_h is passive with respect to the external port ($\dot{\eta}$,F_w).

[4] In this section it is introduced the interconnection between the mechanical and hydraulic subsystems so as to show the passivity property of the interconnected system and that the energy function of the loss-less (without dissipative terms) hydraulic subsystem is non-decreasing. Nevertheless, in the present thesis both subsystems are simulated individually, i.e., the interconnection stage is not used.

[5] The result obtained is the same for the spring-damper model and for the spring-damper-inerter model.

Passivity is characterised by a dissipation inequality which guarantees that the derivative of a storage or energy function is at most the product of the external ports, i.e.,

$$\dot{H}_{pa}(x_m, x_h) \leq \dot{\eta} F_w. \tag{3.65}$$

Taking into account the global energy function given in (3.64), the derivative of the Hamiltonian can be written as

$$\begin{aligned}\dot{H}_{pa}(x_m, x_h) &= \dot{H}_m(x_m) + \dot{H}_h(x_h) \\ &= \frac{\partial H_m}{\partial x_m}^\top (J_m - R_m)\frac{\partial H_m}{\partial x_m} + \frac{\partial H_m}{\partial x_m}^\top \begin{bmatrix} 0 \\ 0 \\ F_w \\ F_p \end{bmatrix} + \frac{\partial H_h}{\partial x_h}^\top (\sigma J_h - \sigma R_h)\frac{\partial H_h}{\partial x_h} + \frac{\partial H_h}{\partial x_h}^\top \begin{bmatrix} 0 \\ \frac{\sigma^2}{I} P_s \end{bmatrix} \\ &= -d(\dot{\eta} - \dot{q})^2 + \dot{\eta} F_w + \dot{q} F_p - \sigma R Q^2 - \sigma \frac{\rho}{Ac^2} Q^3 + \sigma^2 P_s Q.\end{aligned} \tag{3.66}$$

Substituting the interconnection given in (3.62) leads to

$$\begin{aligned}\dot{H}_{pa} &= -d(\dot{\eta} - \dot{q})^2 + \dot{\eta} F_w - \dot{q}\sigma A_c P_s - \sigma R Q^2 - \sigma \frac{\rho}{Ac^2} Q^3 + \sigma P_s A_c \dot{q} \\ &= -d(\dot{\eta} - \dot{q})^2 + \dot{\eta} F_w - \sigma R Q^2 - \sigma \frac{\rho}{Ac^2} Q^3 \leq \dot{\eta} F_w.\end{aligned} \tag{3.67}$$

Since d, R and $Q \geq 0$, it can be concluded that the PA system is passive with respect to the external port ($\dot{\eta}$,F_w). Note that $\dot{H}_{pa}$ has three dissipative terms, the first one due to the damping effects in the mechanical subsystem and the other two due to the dissipative terms in the hydraulic subsystem. It can be noticed that the dissipative terms from the hydraulic subsystem appear multiplied by σ, meaning that this dissipation is decoupled whenever the buoy-piston is disengaged during the downward movement.

In addition, it can be seen that, disregarding the resistive terms, the energy function is non-decreasing, which verifies the storage of the kinetic energy from the mechanical subsystem as potential energy. The derivative of the Hamiltonian function $H_h(x_h)$ is given by

$$\dot{H}_h = \frac{\partial H_h}{\partial x_h}^\top (\sigma J_h - \sigma R_h)\frac{\partial H_h}{\partial x_h} + \frac{\partial H_h}{\partial x_h}^\top \begin{bmatrix} 0 \\ \frac{\sigma^2}{I} P_s \end{bmatrix} = -\sigma R Q^2 - \sigma \frac{\rho}{Ac^2} Q^3 + \sigma^2 P_s Q, \tag{3.68}$$

which due to the switching coupling becomes

$$\dot{H}_h = \begin{cases} -RQ^2 - \frac{\rho}{Ac^2} Q^3 + P_s Q & \text{for } \dot{q} > 0 \\ 0 & \text{otherwise.} \end{cases} \tag{3.69}$$

Hence, without the dissipative terms RQ^2 and $\frac{\rho}{Ac^2} Q^3$, the Hamiltonian function is non-decreasing.

3.3 Results

In this section, it is presented the numerical simulations for the mechanical and hydraulic subsystems. These systems have been simulated separately, therefore the interconnection stage still needs to be included in order to obtain the complete PA interconnected system.

3.3.1 Mechanical subsystem

Tables 3.1, 3.2 and 3.3 summarize the model parameters used for the simulation[6].

Table 3.1: Mechanical model parameters

Parameter	Value	Description	Unit
–	7x7x2	Dimensions floater	m^3
g	9,81	Gravitational acceleration	m/s^2
ρ_{sw}	1025	Sea water density	kg/m^3
m_1	$6{,}27{\cdot}10^5$	Displaced water eq. mass	kg
m_2	1650	Buoy-piston eq. mass	kg
m_a	$1{,}55{\cdot}10^5$	Added mass	kg
d	$2{,}17{\cdot}10^4$	Damping coefficient	Ns/m
D_b	1	Draft	m
k_{PTO}	$5{,}8{\cdot}10^4$	Stiffness of PTO	N/m
d_{PTO}	$1{,}1{\cdot}10^4$	Damping of PTO	Ns/m
–	500	Depth	m

Table 3.2: Wave parameters

Parameter	Value	Description	Unit
H	4	Wave height	m
T	10	Wave period	s
λ_w	156,13	Wave length	m

Table 3.3: Simulation parameters

Description	Value	Unit
Max time step	10^{-3}	s
Solver	ode45	-
Simulation duration	50	s

In Fig. 3.10 it is shown the vertical (heave) displacement of the buoy for the harmonic wave introduced, as well as the excitation force needed to obtain the desired motion of the water body. The initial transients (0 - 10 s) has been removed for clarity.

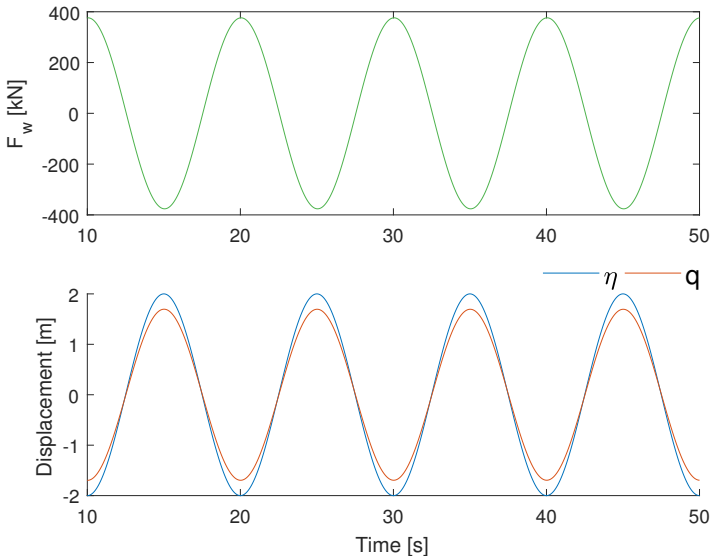

Figure 3.10: Excitation force (top) and wave and buoy displacements (bottom)

[6]It is important to recall that for the simulation of the mechanical subsystem it is considered a spring-damper PTO force instead of the real pumping force derived from the pumping subsystem.

Analysing the evolution of energies involved, in Fig. 3.11 it can be seen the energy transmission between kinetic and potential energies and the total dissipated energy.

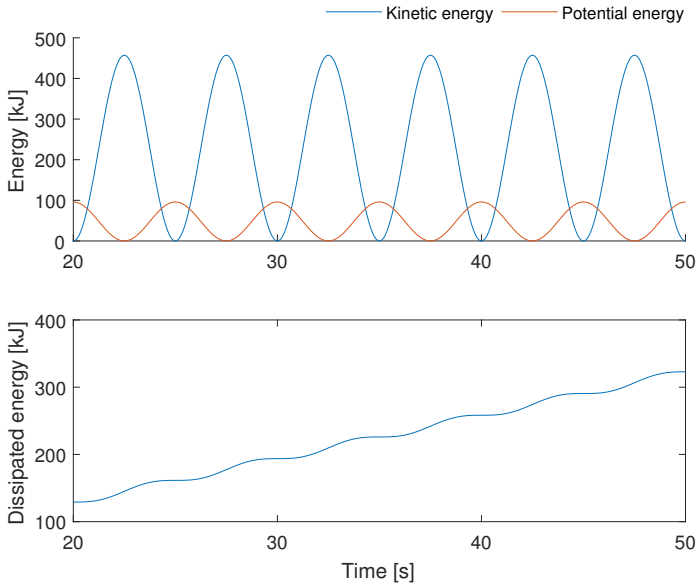

Figure 3.11: Energy evolution

On the other hand, in case of not introducing an external force F_w and with non-null initial position (Fig. 3.12), the energy keeps decreasing due to the dissipative terms.

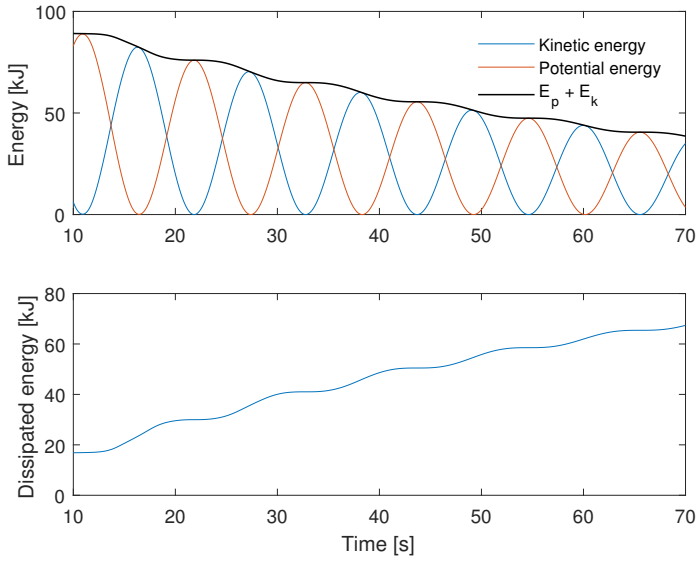

Figure 3.12: Energy evolution for $F_w = 0$

The previous simulation have considered the linearised PTO parameters $k_{PTO} = 5{,}8{\cdot}10^4$ N/m and $d_{PTO} = 1{,}1{\cdot}10^4$ Ns/m. In Fig. 3.13 it is shown the energy dissipated due to the PTO (extracted energy) for different values of the parameters. The results indicate that if increasing k_{PTO} maintaining the value of d_{PTO}, the extracted energy decreases. On the other hand, when the value of k_{PTO} remains the same while increasing d_{PTO}, the value of the absorbed energy increases.

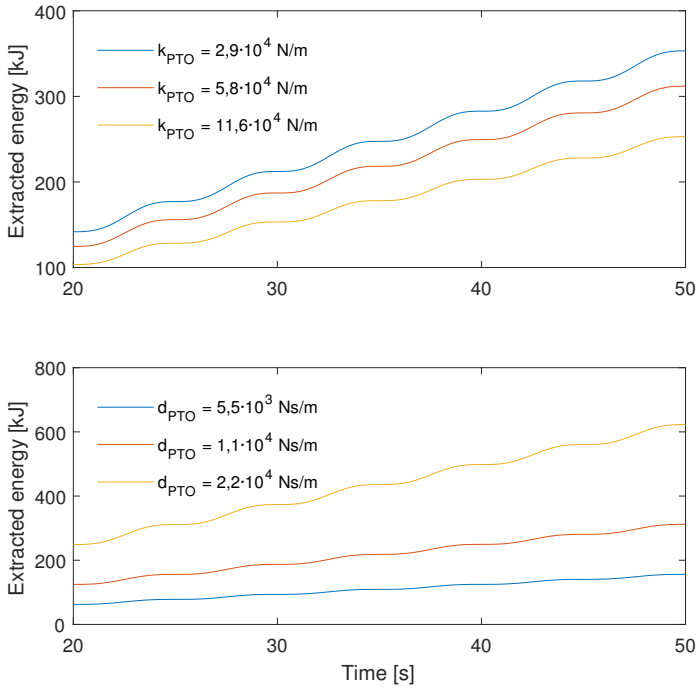

Figure 3.13: Extracted energy for different values of k_{PTO} and d_{PTO}

In the simulation, it has been fixed the motion of the wave and then obtained the corresponding excitation force F_w. However, it would be useful determinate the excitation force required to get the desired displacement of the water mass. Thus, it has been calculated F_w for different wave periods as well as for some wave heights; in Fig. 3.14 is depicted F_w with respect to the force for $H = 1$ m. The results indicate that amplitude of F_w is directly proportional to the wave height; therefore, it is only necessary the value for one wave height and the it can be multiplied by the corresponding factor to obtain F_w. Accordingly, the amplitude of the excitation force is plotted against the wave frequency for a range from 4 to 20 seconds and 1 m height (Fig. 3.15).

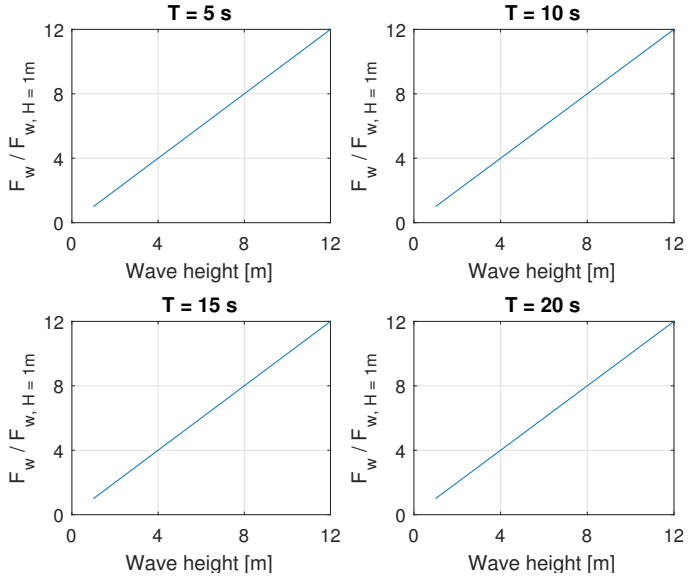

Figure 3.14: Wave excitation force F_w for different wave periods and heights

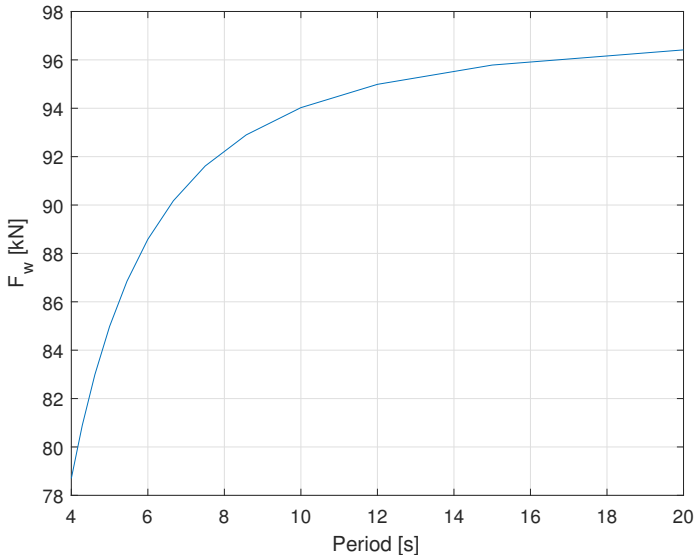

Figure 3.15: Wave excitation force F_w for $H = 1$ m

In order to analyse the result obtained, it is compared the RAO (Response Amplitude Operator) with the results from validated models (a time-domain (TD) and a frequency-domain (FD) models) for a wave period range from 3 to 10 seconds (Fig. 3.16). The parameters used are the same than in (Yu, 2017). In the upper plot it is presented the RAO for the TD and FD models, as well as for the present model using the excitation force F_e obtained from Nemoh and the calculating it through Equation (3.5). In the lower plot, it is depicted the error between the present model (using the F_e equation) and the FD model.

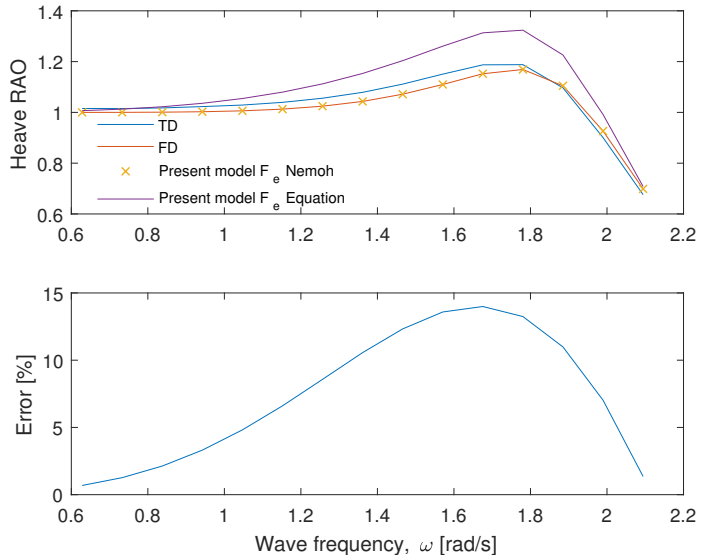

Figure 3.16: Single floater heave RAO

The present model with F_e from Nemoh and the FD results are in good agreement; thus, the inclusion of additional degrees of freedom in the floater does not significantly influence the heaving motion of a single floater. On the other hand, as seen in Fig. 3.1, the deviation of the present model with F_e from the equation increases for high period waves, whereas for lower frequency values (not presented in the figure), the result is similar.

3.3.2 Hydraulic subsystem

Tables 3.4, 3.5 and 3.6 summarize the model parameters used. As the pumping system is simulated individually, it has been fixed a sinusoidal motion to the piston. In this work it has been considered a fixed value of the piston area A_c; however, A_c could be modified to optimize the energy extraction, as done in (Barradas-Berglind et al., 2016b).

Table 3.4: Hydraulic model parameters

Parameter	Value	Description	Unit
g	9.81	Gravitational acceleration	m/s^2
ρ	1080	Working fluid density	kg/m^3
μ	0,0734	Working fluid viscosity	Pas
L_{16}	100	Pipe length	m
A_u	49	Upper reservoir area	m^2
A_l	49	Lower reservoir area	m^2
A_c	0,0738	Cylinder cross section area	m^2
L_{U0}	10	Upper reservoir initial hydraulic head	m
L_{L0}	30	Lower reservoir initial hydraulic head	m

Table 3.5: Piston motion parameters

Parameter	Value	Description	Unit
H	4	Motion height	m
T	10	Period	s

Table 3.6: Simulation parameters

Description	Value	Unit
Max time step	10^{-2}	s
Solver	ode45	-
Simulation duration	40	s

The piston displacement and velocity, pumping force F_p and pumping power $P_p = F_p\dot{q}$ are plotted in Fig. 3.17.

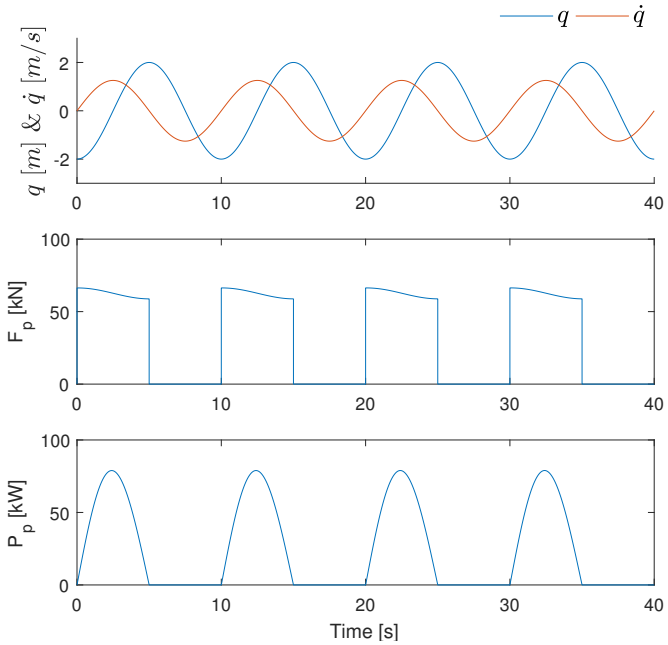

Figure 3.17: Piston displacement and velocity, pumping force and pumping power

In Fig. 3.18 it is plotted the individual contribution to the pumping force of the additional terms described in 3.1.4, implying an increase in the pumping force required at certain points. In the case of the third term, the difference is mainly due to the fact that combining a restistor-inertor with the same length as done in the present model implies that the inertance used is half of the one if only considering an inertor, rather than the effect of the resistor.

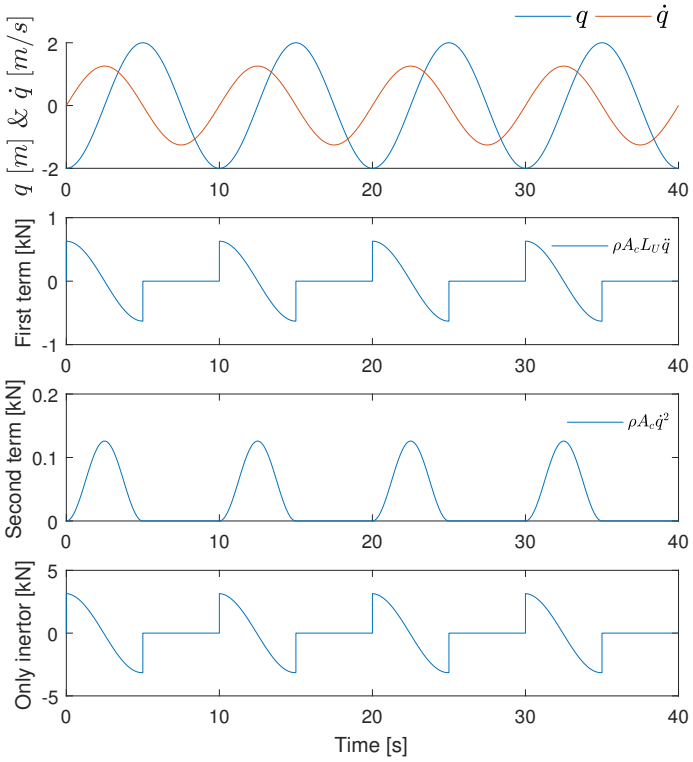

Figure 3.18: Pumping force terms

It can be noticed that the values are small for the simulation parameters used. Nevertheless, the first and second terms can increase its importance depending on the amplitude of the piston motion and the wave frequency. For example, in case of having a 12m height and a period of 4s, the error would be around 9% and 10%, respectively. Moreover, the second term also becomes higher with the increasing of the upper reservoir hydraulic head.

In Fig. 3.19, it is shown the flow rate and pressure difference between the reservoirs, as well as the (maximum) hydraulic head. As would be expected, the pressure increases in the upper reservoir while decreases in the lower by an amount corresponding to the pumped fluid. The hydraulic head increases by 12mm per cycle. This transfer of working fluid from the lower to the upper reservoir is translated into the accumulation of potential energy, as depicted in Fig. 3.20.

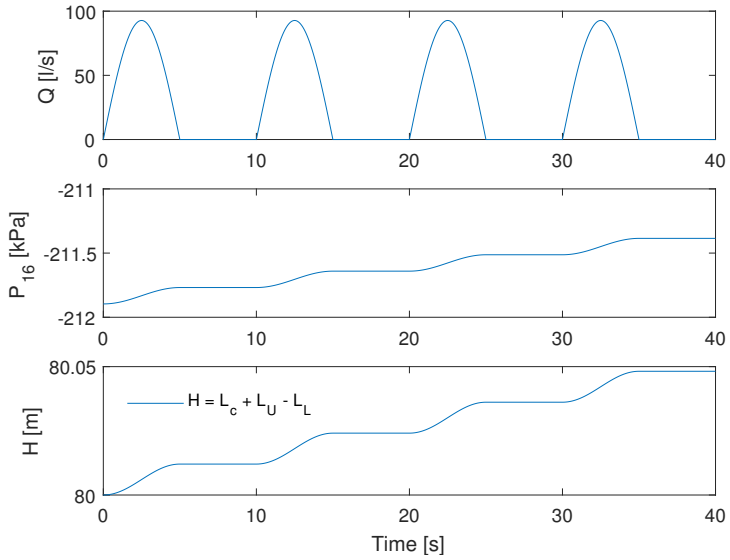

Figure 3.19: Flow rate, pressure difference between reservoirs and hydraulic head

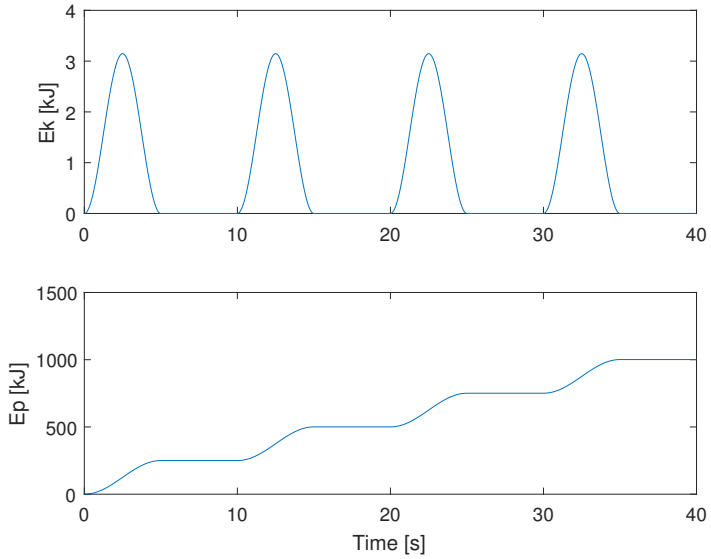

Figure 3.20: Kinetic and potential energies

The pumping and and potential power are close in amplitude, as shown in Fig. 3.21, with the deviation being attributable to the dissipation in the resistors, the change in momentum of the fluid and the kinetic power.

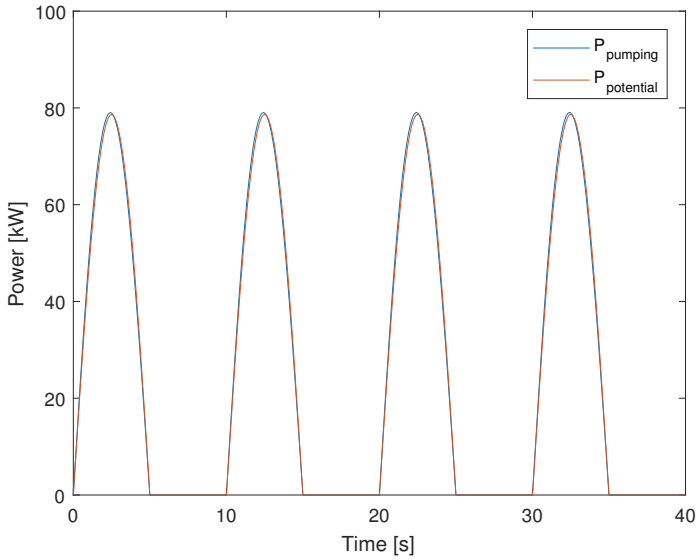

Figure 3.21: Pumping and potential power

The deviation between the pumping and potential energies yields the efficiency of the pumping system

$$\eta[\%] = \frac{E_{potential}}{E_{pumping}} \times 100 = 99,72\%. \tag{3.70}$$

Chapter 4

Array of point absorbers model

A single floater can only extract limited amount of energy, whereas a grid of interconnected floater elements (floater blanket) can sequentially extract more energy in total. Energy extraction is expected to diminish the energy content and height of the wave as it moves through the WEC, i.e., the first pump unit can potentially extract more energy than the second, and so on.

4.1 Model considered

In the case of a floater blanket, the extracted energy of a WEC is not only determined by the incident wave, but also by the radiated/diffracted waves from neighbouring PAs. The schematic of the array of PAs is shown in Fig. 4.1. The water elements are interconnected to its respective neighbours and each pumping system is connected between the same reservoirs. The interconnection force between the water bodies is transmitting the excitation force and the radiation forces coming from the other point absorbers.

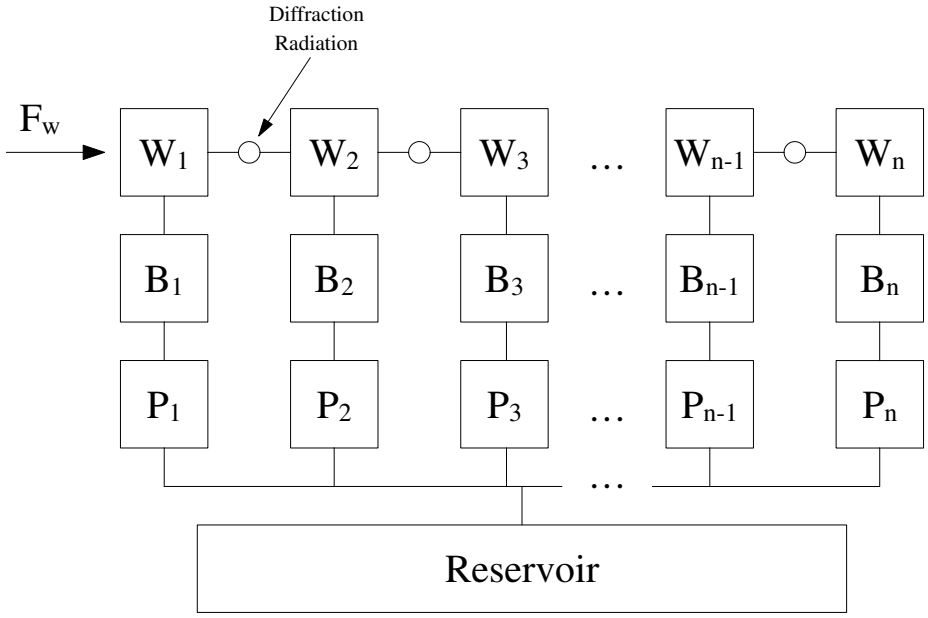

Figure 4.1: Complete PTO schematic

Forces acting on each water body are depicted in Fig. 4.2, for the case of 3 PAs.

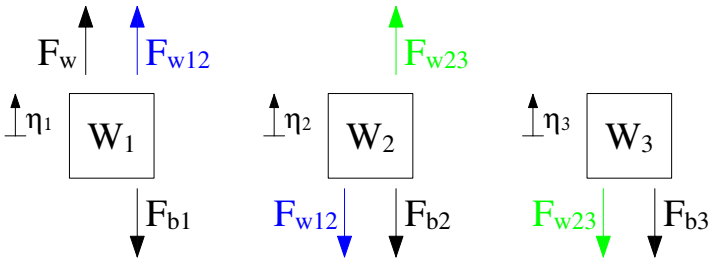

Figure 4.2: Free body diagrams of the water bodies for 3 PAs

Equivalently, it can be expressed for the general case of n point absorbers as

$$\begin{cases} m_1\ddot{\eta}_1 = F_w + F_{b1} + F_{w12} \\ m_1\ddot{\eta}_2 = F_{b2} - F_{w12} + F_{w23} \\ \quad\vdots \\ m_1\ddot{\eta}_n = F_{bn} - F_{w(n-1,n)} + \cancel{F_{\cdot}}. \end{cases} \tag{4.1}$$

Note that reflection term is neglected in the last equation.

The interconnection force between water bodies i and j can be defined with position and velocity contributions as[1]

$$F = \rho_1 * k_1 \left(\eta_j - \eta_i\right) + \rho_2 * k_2 \left(\dot{\eta}_j - \dot{\eta}_i\right), \tag{4.2}$$

where ρ_1, k_1, ρ_2 and k_2 are parameters and the operator $*$ represents the convolution operation. Defining ρ_1 and ρ_2 as

$$\rho_1 = e^{-\lambda_1 t}, \quad \rho_2 = e^{-\lambda_2 t} \tag{4.3}$$

and applying the Laplace transform to (4.2) yields

$$F(s) = \underbrace{\frac{1}{s+\lambda_1}}_{H_1(s)} k_1 \left(\eta_j(s) - \eta_i(s)\right) + \underbrace{\frac{1}{s+\lambda_2}}_{H_2(s)} k_2 \left(\dot{\eta}_j(s) - \dot{\eta}_i(s)\right), \tag{4.4}$$

where s is the Laplace variable and $H_1(s)$, $H_2(s)$ are first order lowpass filters.

Hence, the interconnection force F_{wij} between water bodies i and j is given by

$$F_{wij} = \alpha_{ij} + \beta_{ij}, \tag{4.5}$$

where α_{ij} and β_{ij} are dynamical varying variables that depend on the parameters $\lambda_{\alpha,ij}$, $k_{\alpha,ij}$, $\lambda_{\beta,ij}$ and $k_{\beta,ij}$ satisfying Equation (4.6). These parameters have to be identified in order to approximate the connection between the PAs.

$$\dot{\alpha}_{ij} = -\boldsymbol{\lambda_{\alpha,ij}}\alpha_{ij} + \boldsymbol{k_{\alpha,ij}}(\eta_j - \eta_i) \tag{4.6a}$$

$$\dot{\beta}_{ij} = -\boldsymbol{\lambda_{\beta,ij}}\beta_{ij} + \boldsymbol{k_{\beta,ij}}(\dot{\eta}_j - \dot{\eta}_i). \tag{4.6b}$$

[1] Convolution kernels given by Cummins' equation.

4.2 Reference model

4.2.1 Formulation

To adjust the parameters of the model, it is needed a verified model to compare with. Hence, a time-domain model has been developed from (Wei et al., 2017b) and subsequently validated against the results from it. The present model only takes into account the heave motion (vertical displacement) and does not consider mechanical coupling between the floaters. Based on this assumptions, the motion equations for a floater blanket of M elements, where the index m represents the m^{th} floater, are described by

$$M^{(m)}\ddot{X}^{(m)} = F_e^{(m)} + F_r^{(m)} + F_{hs}^{(m)} + F_{pto}^{(m)}, \tag{4.7}$$

where $M^{(m)}$ is the mass of the buoy m, $X^{(m)}$ is the displacement of each buoy, $F_e^{(m)}$ is the wave excitation force vector, $F_r^{(m)}$ is the radiation force vector, $F_{hs}^{(m)}$ is the restoring force vector and $F_{pto}^{(m)}$ is the force vector coming from the hydraulic system.

The radiation force $F_r^{(m)}$ is composed of the radiation forces due to the motion of the floater m itself as well as to the other floaters:

$$F_r^{(m)} = -\sum_{n=1}^{M}(A^{(m,n)}\ddot{X}^{(m)} + C^{(m,n)}\dot{X}^{(m)}), \tag{4.8}$$

where $A^{(m,n)}$, $C^{(m,n)}$ are the frequency-dependent added-mass and damping coefficient matrices, respectively. Note that the superscripts m and n denote the radiation contribution of floater n on floater m. Thus, in this model the neighbour radiation is considered as a superposition of the effects due to the motion of the other floaters.

In addition, $F_{hs}^{(m)}$ is defined as a linear function of the heave motion, which can be expressed as

$$F_{hs}^{(m)} = -K_{hs}^{(m)}X^{(m)}, \tag{4.9}$$

where $K_{hs}^{(m)}$ corresponds to the hydrostatic stiffness that specifies the variation of the net weight and buoyancy load with respect to the changes in position from equilibrium.

Finally, a simple PTO is considered[2], described as a linear spring-damper system by

$$F_{pto}^{(m)} = -K_{pto}^{(m)}X^{(m)} - C_{pto}^{(m)}\dot{X}^{(m)}, \tag{4.10}$$

where K_{pto} and C_{pto} are the stiffness and damping coefficients of the PTO, respectively. Therefore, we have the following equation

$$M^{(m)}\ddot{X}^{(m)} = F_e^{(m)} - \sum_{n=1}^{M}(A^{(m,n)}\ddot{X}^{(m)} + C^{(m,n)}\dot{X}^{(m)}) - K_{hs}^{(m)}X^{(m)} + F_{pto}^{(m)}. \tag{4.11}$$

A ramp function R_f is used to introduce the wave excitation force in order to avoid strong transient flows at earlier time steps of the simulation. The ramp function is given by

$$R_f = \begin{cases} \frac{1}{2}(1+\cos(\pi+\frac{\pi t}{t_r})) & \frac{t}{t_r} < 1 \\ 1 & \frac{t}{t_r} \geq 1 \end{cases} \tag{4.12}$$

where t is the simulation time and t_r is the ramp time.

[2]In (Wei et al., 2017b), it is also considered a spring-damper PTO.

The time-averaged absorbed power can be obtained integrating the extracted power for one wave period at steady state or, assuming a sinusoidal velocity of the floater, it can be calculated with

$$P_k = \frac{1}{2} C_{pto,k} |\dot{X}_k|^2, \tag{4.13}$$

where P_k is the time-averaged absorbed power by the floater k, C_{pto} is the damping coefficient of the floater k in the PTO system and $|\dot{X}_k|$ is the amplitude of the heave velocity of the floater k.

4.2.2 Results

The relevant parameters of the model are summarized in Table 4.1. It is considered a one-column floater blanket comprised of ten prismatic buoys.

Table 4.1: Floater blanket parameters

Description	Value	Unit
Number of floaters	10	-
Dimension of floater	7x7x2	m^3
Mass of floater	1500	kg
Stiffness of PTO	$5{,}8 \cdot 10^4$	N/m
Damping of PTO	$1{,}1 \cdot 10^4$	Ns/m
Water density	1025	kg/m^3
Draft	1	m

Similarly to the PA, the hydrodynamic coefficients required for the model $-A,\ C,\ F_e-$ can be obtained from Nemoh (Wei et al., 2017b). The floater blanket displacement for a wave height of 2 m and four wave periods is shown in Fig. 4.3. The maximum displacement of each buoy along the floater blanket is indicated by a black line.

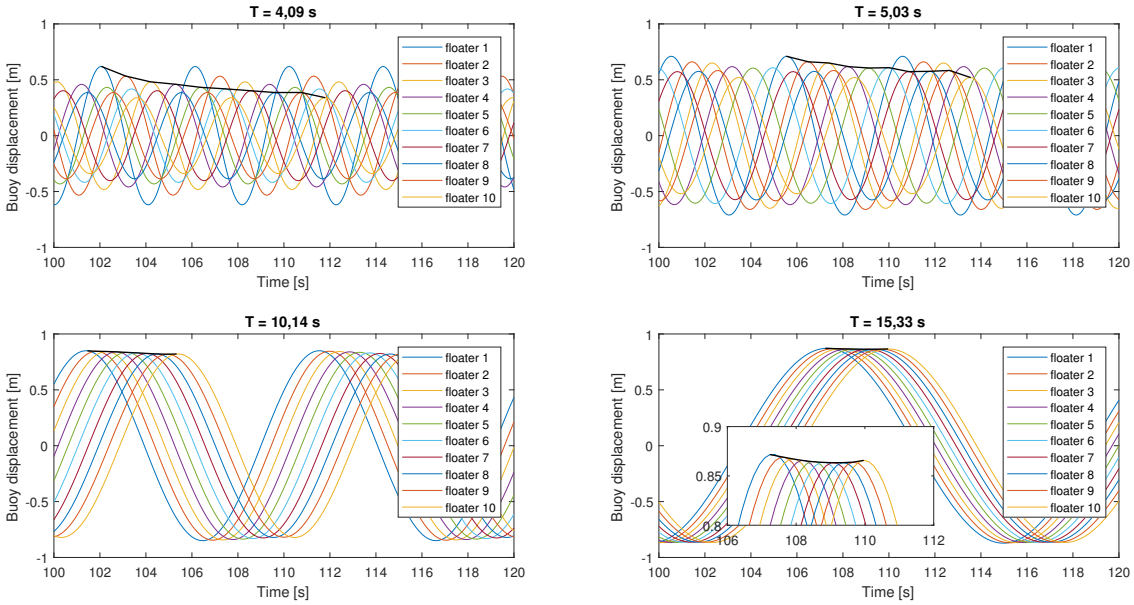

Figure 4.3: Buoy displacement for different frequencies

The amplitude of the floaters displacement is always less than 1 and decreases with the wave frequency. For low frequency waves, the floaters moves synchronously with the wave evolution, such that all the floater elements exhibits a similar performance. Therefore, the energy extraction for each unit is similar. On the other hand, for short-period waves, there is a general decreasing trend of the amplitude from the first floater to the last. This is because the diffraction and radiation effects become significant when the length of the floater blanket is comparable to the wavelength.

From these results, it can be calculated the overall capture power of the whole floater blanket. In Fig. 4.4, it is shown the result for the 1 DOF case (only considering heave degree of freedom) and for the 2 DOF case[3] (taking into account heave and pitch motion). Additionally, it is plotted the results of some cases from (Wei et al., 2017b). These cases are briefly described below[4]:

- **TD** is the time-domain model (Wei et al., 2017a), based on the open-source WEC-Sim code.
- **case1 FD** is the frequency-domain general case.
- **case2 FD** neglects the neighbour radiation.
- **case3 FD** removes the hinges between the floater elements, but restricts their surge motion individually (each floater has independent heave and pitch motions).
- **case5 FD** is similar to case3, but does not account for the neighbour radiation. The floater elements are considered as independent heave absorbers.

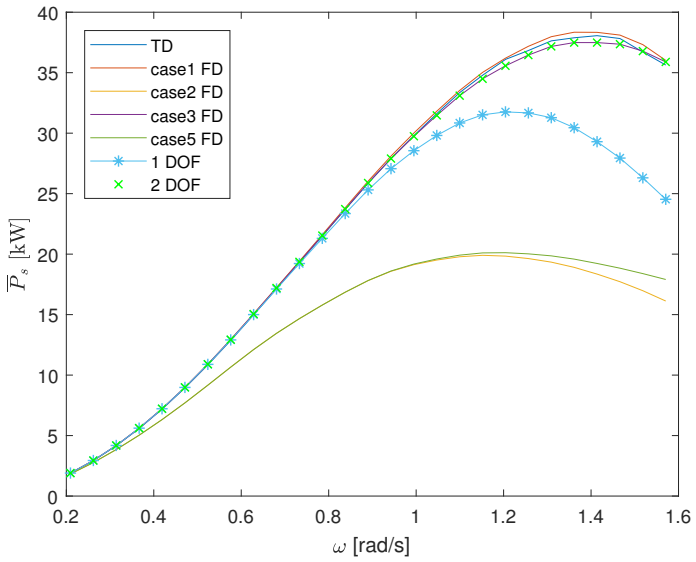

Figure 4.4: Overall capture power [kW]

It can be seen that the power capture of the floater blanket increases with wave frequency, reaching the maximum energy extraction at $\omega \approx 1{,}4$ rad/s. The results indicate that not considering hinge coupling between floaters does not significantly influence the overall capture power for the simulation parameters considered. Therefore, in this case, if restricting each surge displacement individually or only fixing the surge motion of the first floater, results in a similar motion of the floater blanket. However, when considering different PTO settings for each point absorber, the hinge coupling may be more relevant.

[3]The inertia and stiffness coefficients used are the same than in (Yu, 2017).
[4]The numbering of the cases is the same than in (Wei et al., 2017b).

On the other hand, if heave and pitch motion are taken into account (2 DOF), the result is almost equal to case3. Finally, there is a great reduction of the overall extracted power for 1 DOF case compared with 2 DOF for high frequency waves, though for low frequencies the match is perfect. Thus, not considering pitch motion may underestimate the capture power by $46,3\%$ at maximum frequency. In terms of overall capture power, radiation becomes more important as wave frequency increases and so does the radiation due to the pitch motion. The individual capture power in each floater for the 1 DOF and 2 DOF cases is presented in Fig. 4.5.

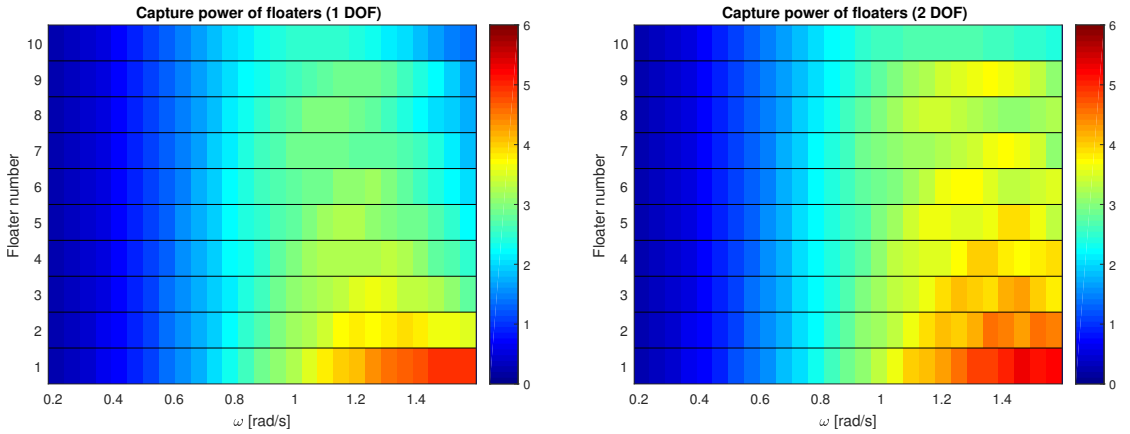

Figure 4.5: Capture power [kW] only considering heave (left) and taking into account heave and pitch (right)

The radiation terms represent an energy redistribution along the floater blanket due to the motion of the floaters. The superposition of radiated/diffracted waves may strengthen or diminish the waves at the location of the floaters, resulting in an increase or decrease of energy extraction on those floaters.

4.3 Parameter identification

From the 1 DOF model, it can be determined the parameters for the interconnection of the PAs; the procedure is shown in the following. First, it has been extracted the displacement, velocity and acceleration of each floater for a wave of 1 m height and a frequency of 0,62 rad/s (T = 10,14s).

From this data, it has to be obtained individually for each point-absorber the height and phase of the equivalent wave that would produce the desired motion of each floater. First, it can be defined an equivalent force due to the superposition of the motion of the wave body itself and the radiated waves coming from the other wave bodies. Thus, Equation (4.11) can be rewritten as

$$\left[M^{(m)} + A^{(m,m)}\right] \ddot{X}^{(m)} + C^{(m,m)} \dot{X}^{(m)} = \underbrace{F_e^{(m)} - \sum_{\substack{n=1 \\ n \neq m}}^{M} \left(A^{(m,n)} \ddot{X}^{(m)} + C^{(m,n)} \dot{X}^{(m)}\right)}_{F_{e,eq}^{(m)}} + F_{hs}^{(m)} + F_{pto}^{(m)}. \tag{4.14}$$

Secondly, from this equivalent force $F_{e,eq}^{(m)}$, it can be calculated the corresponding height and phase of the equivalent wave from the excitation force presented in the previous chapter:

$$F_e = \left(m_a \ddot{\eta}^* + B\dot{\eta}^* + K\eta^*\right).$$

The final result is shown in Fig. 4.6. The dashed lines represent the displacement of the water elements and the solid lines correspond to each buoy displacement. For better clarity, each pair wave-floater are plotted with the same colour. Once known the wave and floaters motion, it can be recovered the excitation force that should be introduced to each wave body with Equations (3.22) and (4.1).

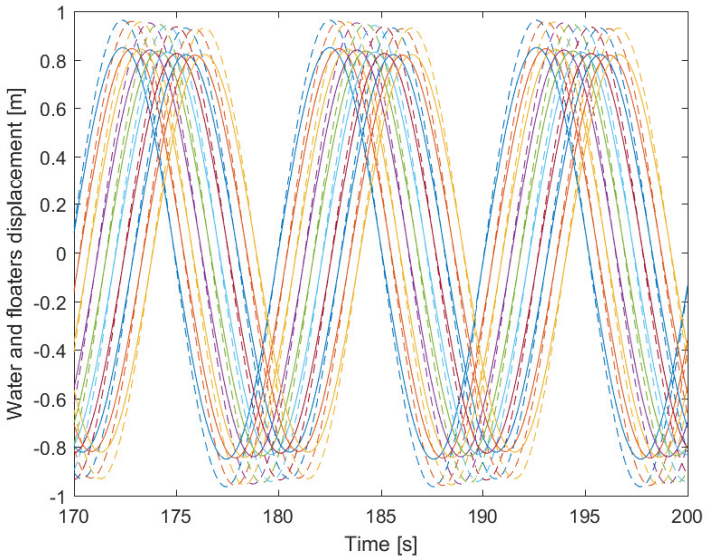

Figure 4.6: Waves (dashed lines) and floaters displacement

From this point, the parameters of the connection between the PAs can be calculated through an optimization method[5]. In the case of the last couple of floaters, we have $F_{w9,10}$ defined as

$$F_{w9,10} = \alpha_{9,10} + \beta_{9,10},$$

and taking into account the expressions of the variables $\alpha_{9,10}$ and $\beta_{9,10}$:

$$\dot{\alpha}_{9,10} = -\boldsymbol{\lambda_{\alpha(9,10)}}\ \alpha_{9,10} + \boldsymbol{k_{\alpha(9,10)}}\ (\eta_{10} - \eta_9)$$
$$\dot{\beta}_{9,10} = -\boldsymbol{\lambda_{\beta(9,10)}}\ \beta_{9,10} + \boldsymbol{k_{\beta(9,10)}}\ (\dot{\eta}_{10} - \ \dot{\eta}_9),$$

the best estimation of the parameters is

$$\lambda_{\alpha(9,10)} = 0,018\ s^{-1} \qquad k_{\alpha(9,10)} = 2440,626\ \frac{N}{ms} \qquad \lambda_{\beta(9,10)} = 3,415\ s^{-1} \qquad k_{\beta(9,10)} = 3,864{\cdot}10^6\ \frac{N}{m}.$$

The error between the results from the reference model and the displacement calculated using the above parameters for a time step of 10^{-3} s is depicted in Fig. 4.7. In this case, the contribution of α to the interconnection force is very small compared to β (see Fig. 4.8).

[5]The related MATLAB code can be found in the Appendix.

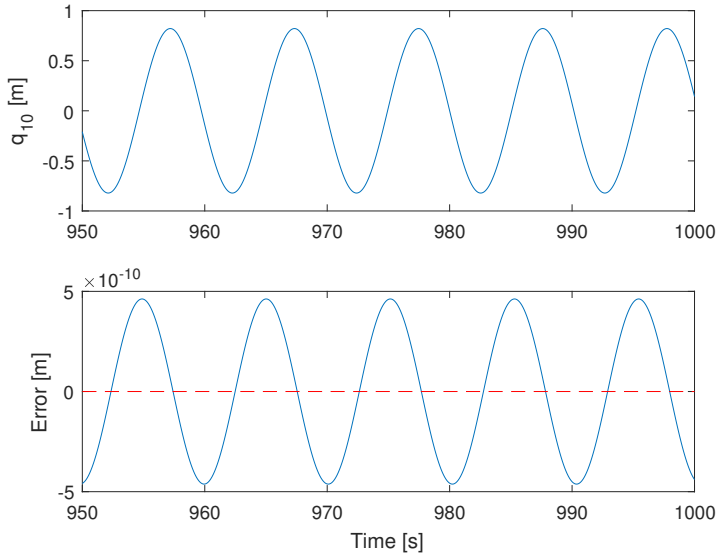

Figure 4.7: Floater 10 displacement and error

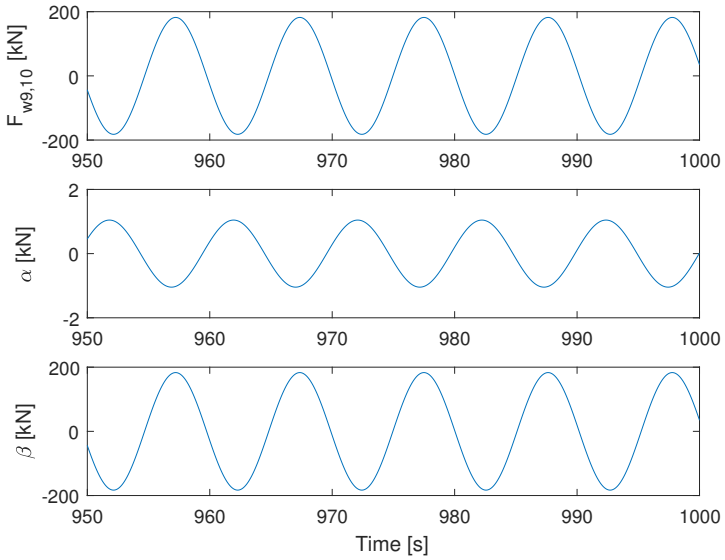

Figure 4.8: Interconnection force between PAs 9 and 10

Therefore, as the deviation is negligible, the interconnection proposed between water bodies with the parameters found acquires an excellent result. However, these connection between the water elements and the parameters that define it should be evaluated for other simulation conditions (incoming wave height and frequency, PTO settings, etc.) in order to verify the correct concept used in the present model[6]. Hence, further investigation will be required.

[6]Since the coefficients that define the radiation force are frequency-dependent, the parameters obtained for the present model may also depend on the wave frequency.

Chapter 5

Conclusions and further work

5.1 Conclusions

The goal of this was to develop a model of the MP^{2}PTO system with improved computational efficiency. First, a reduced and modular model for the buoy-piston-pump point-absorber system has been presented. The model takes into account the radiation effects with software based on the boundary-element method. Besides, the simulations of both mechanical and hydraulic subsystems have shown good individual performance and the inerter has successfully been incorporated in the mechanical subsystem. Regarding the pumping system, the additional terms introduced has proven to have small impact for the simulation conditions utilized; nevertheless, its contribution can increase and should therefore be investigated. In addition, it has been compared the present results of the mechanical subsystem with those from a time-domain and a frequency-domain validated models, showing the main deviations for high frequency values.

Subsequently, the point absorber is described in the port-Hamiltonian framework and it is shown the passivity of the interconnected system with respect to its external port and the effectively storage of potential energy. The PH framework provides a cross-domain energy-based modelling methodology that allows for modularity and scalability. Moreover, the role of energy and the interconnection between subsystems provide the basis for control, which is interesting in particular for complex non-linear systems.

Furthermore, the model for an array of point-absorber devices is introduced. From the analysis of the reference model results, it can be concluded that the floater elements exhibit a similar response for long-period waves, but their motion may be influenced by diffraction and radiation effects under short-period waves. It is also shown that the effect of pitch becomes important for short-period waves; moreover, if mechanical coupling is introduced, this degree of freedom will have to be considered. On the other hand, the results indicate that not considering hinge coupling between floaters does not significantly influence the overall capture power for the simulation parameters considered. Lastly, in terms of overall capture power, the 2 DOF simulated model produce similar results to the 6 DOF frequency model from (Wei et al., 2017b).

Finally, the interconnection of several point-absorber devices through the water bodies is proposed and tested, obtaining a perfect match with the reference model for the simulation conditions employed.

5.2 Recommendations

Future work still needs to be done to obtain a complete model of the WEC in the PH framework. Some further steps could be:

1. Include the varying hydraulic head term in the hydraulic subsystem.
2. Connect the mechanical and hydraulic subsystems to simulate the real system instead of a spring-damper PTO. As explained in the thesis, the interconnection proposed does not follow the usual input-output linkage and incorporating it would therefore require further work.
3. Estimate all the parameters from the interconnection of the ten floater elements and evaluate the interconnection for different simulation conditions.
4. Include the proposed interconnection model into the PH framework.
5. Evaluate the model for all range of wave frequencies.
6. Include mechanical coupling between the floaters. This joints and the forces involved have to be defined and modelled.
7. Design of control strategies, by modifying the cylinder area, in order to maximize the extracted energy.

Bibliography

Barradas-Berglind, J., Munoz-Arias, M., Wei, Y., Prins, W., Vakis, A., and Jayawardhana, B. Towards Ocean Grazer's Modular Power Take-Off System Modeling: a Port-Hamiltonian Approach. In *20th IFAC World Congress*, 2016a.

Barradas-Berglind, J.J., Meijer, H., van Rooij, M., Clemente-Piñol, S., Galván-García, B., Prins, W.A., Vakis, A.I., and Jayawardhana, B. Energy capture optimization for an adaptive wave energy converter. In *Proceedings of the RENEW2016 Conference*, pages 171–178, 2016b.

Clemente Piñol, S. Dynamical modelling, analysis and optimization of a floater blanket for the Ocean Grazer. Master's thesis, University of Groningen, 2015.

EIA Energy Information Administration. Total electricity net generation 2014. Official Energy Statistics from the US Government. Available at https://www.eia.gov.

Falnes, J. *Ocean waves and oscillating systems*. Cambridge University Press, 2002.

Galván García, B. Nonlinear control design for wave energy converter. Master's thesis, University of Groningen, 2014.

IEA International Energy Agency. Ireland - Energy System Overview. Available at https://www.iea.org/media/countries/Ireland.pdf.

Journée, J.M.J. and Massie, W.W. *Offshore hydromechanics*. Delft University of Technology, First edition, 2001.

Kulakowski, B. T., Gardner, J. F., and Shearer, J. L. *Dyanmic modeling and control of engineering systems*. Cambridge University Press, Third edition, 2007.

Martí Saumell, J. Dynamical modelling, analysis and control design of a distributed sea wave energy storage system. Master's thesis, University of Groningen, 2013.

Meijer, H. Simulation of a piston-type hydraulic pump for the Ocean Grazer. Master's thesis, University of Groningen, 2014.

National Renewable Energy Laboratory and Sandia Corporation. Theory - WEC-Sim documentation. Available at https://wec-sim.github.io/WEC-Sim/theory.html.

Observ'ER. The state of renewable energies in europe. EuroObserv'ER Report, 2016.

Ocean Grazer Group. Ocean grazer - A novel ocean energy converter. Available at http://www.oceangrazer.com.

Ringwood, J. V., Bacelli, G., and Fusco, F. Energy-maximizing control of wave-energy converters. *IEEE Control Systems Magazine*, 2014.

Smith, M. C. Synthesis of mechanical networks: the inerter. In *Proceedings of the 41st IEEE Conference on Decision and Control*, volume 2, pages 1657–1662, 2002.

Straume, I. World wave energy resource map. Available at https://commons.wikimedia.org/wiki/File:World_wave_energy_resource_map.png, 2014.

Thorpe, T.W. 2010 survey of energy resources. Technical report, World Energy Council, 2010.

Vakis, A. I. and Anagnostopoulos, J. S. Mechanical design and modeling of a single-piston pump for the novel power take-off system of a wave energy converter. *Renewable Energy*, 2016.

Vakis, A. I., Meijer, H., and Prins, W. A. *First Steps in the Design and Construction of the Ocean Grazer*. ASME/AIAA, 2014.

van der Schaft, A. Port-hamiltonian systems: an introductory survey. In *Proceedings of the International Congress of Mathematicians*, 2006.

van der Schaft, A. and Jeltsema, D. *Port-Hamiltonian Systems Theory: An Introductory Overview*, volume 1. 2014.

van Rooij, M. Experimental validation of dynamical contact models of the Ocean Grazer. Master's thesis, University of Groningen, 2015.

van Rooij, M., Meijer, H., Prins, W.A., and Vakis, A.I. Experimental performance evaluation and validation of dynamical contact models of the ocean grazer. In *OCEANS 2015-Genova*, pages 1–6, 2015.

Wei, Y., Berglind, J.J. Barradas, van Rooij, M., Prins, W.A., Jayawardhana, B., and Vakis, A.I. Investigating the adaptability of the multi-pump multi-piston power take-off system for a novel wave energy converter. *Renewable Energy*, 2017a.

Wei, Y., Yu, Z., Berglind, J.J. Barradas, van Rooij, M., Prins, W.A., Jayawardhana, B., and Vakis, A.I. A frequency-domain model for a novel wave energy converter. In *European Wave and Tidal Energy Conference Series (EWTEC)*, 2017b.

Yu, Z. Hydrodynamic analysis of the floater blanket in the frequency domain. Master's thesis, University of Groningen, 2017.

Appendix A

MATLAB code

In the following it is provided the PH model code and simulink models for the mechanical and hydraulic subsystems, as well as the code and simulink model for the array of point-absorbers.

A.1 Mechanical subsystem

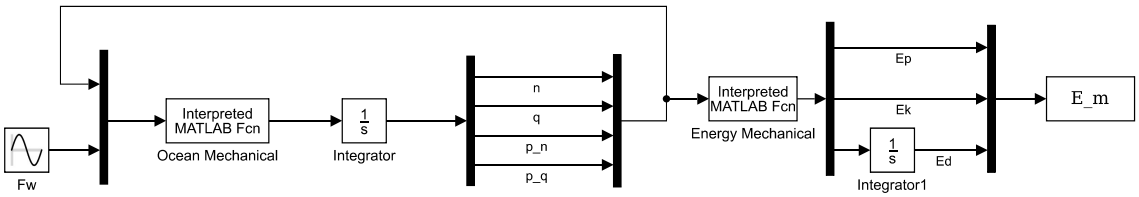

Figure A.1: Mechanical model in Simulink

A.1.1 Spring-damper model

```
function [dx_m]= Ocean_Mechanical(w)
    n   = w(1);
    q     = w(2);
    p_n = w(3);
    p_q   = w(4);
    Fw   = w(5);

    % Parameters
    g = 9.81; % Gravitational acceleration [m/s$^2$]
    rho_sw = 1025; % Sea water density [kg/m$^3$]
    Aw = 49; % Water area 7x7 [m$^2$]
    k = Aw*rho_sw*g; % Stiffness (Buoyancy coefficient) [kg/s$^2$]
    T = 10;
    w = 2*pi/T; % Incoming wave frequency [rad/s]
    ma = 1.553425e5; % Added mass [kg]
    d = 2.167722e4; % Damping coefficient [Ns/m]
```

```
    k = k - ma*w^2; % Stiffness coefficient [kg/s$^2$]
    kPTO = 5.8e4; % Stiffness of PTO [N/m]
    dPTO = 1.1e4; % Damping of PTO [Ns/m]
    m1 = Aw*rho_sw*g/(2*w^2); % Water mass [kg]
    m2 = 1500+150; % Buoy-piston mass [kg]

    % Pumping force
    Fp = -kPTO*q - dPTO*p_q/m2;

    %Partial derivatives of the Hamiltonian Hm(x_m)
    %with x_m = [n, q, p_n, p_q]'
    dHm_dn   = k*(n-q);
    dHm_dq   = -k*(n-q);
    dHm_dp_n = p_n/m1;
    dHm_dp_q = p_q/m2;

    %Damping matrix
    D_m = [d -d;
         -d  d];

    %Interconnection Matrix
    J_m = [zeros(2), eye(2);
         -eye(2), zeros(2)];

    %Dissipation matrix
    R_m = [zeros(2), zeros(2);
         zeros(2), D_m];

    %Partial derivatives of Hamiltonian
    dH_dx_m=[dHm_dn  ;...
             dHm_dq    ;...
             dHm_dp_n;...
             dHm_dp_q  ];

    %Input matrix
    G_m=[zeros(2);
         eye(2)];

    %Inputs of the mechanical subsystem
    u_m = [Fw;
           Fp];

    %Port-Hamiltonian System dynamics
    dx_m = (J_m-R_m)*dH_dx_m + G_m*u_m;
end
```

```
function [E_m]= Energy_Ocean_Grazer_Mechanical(w)
    n   = w(1);
    q     = w(2);
    p_n = w(3);
    p_q   = w(4);

    % Parameters
    g = 9.81; % Gravitational acceleration [m/s$^2$]
    rho_sw = 1025; % Sea water density [kg/m$^3$]
    Aw = 49; % Water area 7x7 [m$^2$]
    k = Aw*rho_sw*g; % Stiffness (Buoyancy coefficient) [kg/s$^2$]
    T = 10;
    w = 2*pi/T; % Incoming wave frequency [rad/s]
    ma = 1.553425e5; % Added mass [kg]
    d = 2.167722e4; % Damping coefficient [Ns/m]
    k = k - ma*w^2; % Stiffness coefficient [kg/s$^2$]
    kPTO = 5.8e4; % Stiffness of PTO [N/m]
    dPTO = 1.1e4; % Damping of PTO [Ns/m]
    m1 = Aw*rho_sw*g/(2*w^2); % Water mass [kg]
    m2 = 1500+150; % Buoy-piston mass [kg]

    Potential = 1/2*k*(n-q)^2 + 1/2*kPTO*(q)^2;

    Kinetic = 1/2*p_n^2/m1 + 1/2*p_q^2/m2;

    Dissipated = d*(p_n/m1 - p_q/m2)^2 + dPTO*(p_q/m2)^2;

    E_m = [Potential;...
           Kinetic;...
           Dissipated];

end
```

A.1.2 Spring-damper-inerter model

```
function [dx_m]= Ocean_Mechanical(w)
    eta   = w(1);
    q     = w(2);
    p_eta = w(3);
    p_q   = w(4);
    Fw    = w(5);

    % Parameters
    g = 9.81; % Gravitational acceleration [m/s$^2$]
    rho_sw = 1025; % Sea water density [kg/m$^3$]
    Aw = 49; % Water area 7x7 [m$^2$]
    k = Aw*rho_sw*g; % Stiffness coefficient [kg/s$^2$]
    T = 10;
    w = 2*pi/T; % Incoming wave frequency [rad/s]
    ma = 1.553425e5; % Added mass [kg]
    d = 2.167722e4; % Damping coefficient [Ns/m]
    kPTO = 5.8e4; % Stiffness of PTO [N/m]
    dPTO = 1.1e4; % Damping of PTO [Ns/m]
    m1 = Aw*rho_sw*g/(2*w^2); % Water mass [kg]
    m2 = 1500+150; % Buoy-piston mass [kg]

    M = m1*m2+m1*ma+m2*ma;
    alpha1 = m1*(ma+m2)/M;
    beta1 = ma*m2/M;
    alpha2 = m1*ma/M;
    beta2 = m2*(m1+ma)/M;

    % Pumping force
    Fp = -kPTO*q - dPTO*p_q/m2;

    %Partial derivatives of the Hamiltonian Hm(x_m)
    %with x_m = [\eta, q, p_eta, p_q]'
    dHm_deta   = k*(eta-q);
    dHm_dq     = -k*(eta-q);
    dHm_dp_eta = (p_eta/m1)+ma*(p_eta/m1-p_q/m2)/m1;
    dHm_dp_q   = (p_q/m2)-ma*(p_eta/m1-p_q/m2)/m2;

    %Damping matrix
    D_m = (m1*m2/M)^2*[d -d;
         -d  d];

    %Interconnection Matrix
    J_m=[ zeros(2)  [alpha1 beta1; alpha2 beta2];...
         -[alpha1 beta1; alpha2 beta2]'      zeros(2)];

    %Dissipation matrix
    R_m=[zeros(2)   zeros(2);...
         zeros(2)      D_m];
```

```
    %Partial derivative of Hamiltonian
    dH_dx_m=[dHm_deta  ;...
             dHm_dq    ;...
             dHm_dp_eta;...
             dHm_dp_q  ];

    %Input matrix
    G_m=[zeros(2);
        m1*(m2+ma)/M ma*m1/M;
        m2*ma/M m2*(m1+ma)/M];

    %Inputs of the mechanical subsystem
    u_m = [Fw;...
           Fp];

    %Port-Hamiltonian System dynamics
    dx_m=(J_m-R_m)*dH_dx_m+G_m*u_m;
end
```

```
function [E_m]= Energy_Ocean_Grazer_Mechanical(w)
    n   = w(1);
    q     = w(2);
    p_n = w(3);
    p_q   = w(4);

    % Parameters
    g = 9.81; % Gravitational acceleration [m/s$^2$]
    rho_sw = 1025; % Sea water density [kg/m$^3$]
    Aw = 49; % Water area 7x7 [m$^2$]
    k = Aw*rho_sw*g; % Stiffness coefficient [kg/s$^2$]
    T = 10;
    w = 2*pi/T; % Incoming wave frequency [rad/s]
    ma = 1.553425e5; % Added mass [kg]
    d = 2.167722e4; % Damping coefficient [Ns/m]
    kPTO = 5.8e4; % Stiffness of PTO [N/m]
    dPTO = 1.1e4; % Damping of PTO [Ns/m]
    m1 = Aw*rho_sw*g/(2*w^2); % Water mass [kg]
    m2 = 1500+150; % Buoy-piston mass [kg]

    Potential = 1/2*k*(n-q)^2 + 1/2*kPTO*(q)^2;
    Kinetic = 1/2*p_n^2/m1 + 1/2*p_q^2/m2 + 1/2*ma*(p_n/m1-p_q/m2)^2;
    Dissipated = d*(p_n/m1 - p_q/m2)^2 + dPTO*(p_q/m2)^2;

    E_m = [Potential;...
           Kinetic; ...
           Dissipated];

end
```

A.2 Hydraulic subsystem

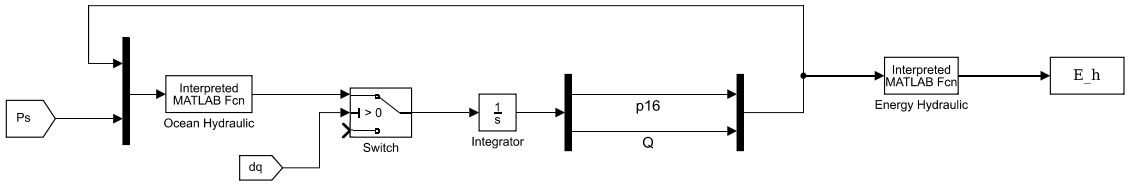

Figure A.2: Hydraulic model in Simulink

```
function dx_h  = Ocean_Hydraulic(w)
    p16 = w(1);
    Q = w(2);
    Ps = w(3);

    % Parameters
    g = 9.81; % Gravitational acceleration [m/s2]
    rho = 1080; % Fluid density [kg/m3]
    mu = 0.0734; % Fluid viscosity [Ns/m2]
    Lc = 100; % Pipe length [m]
    Au = 49; % Upper reservoir area [m2]
    Al = 49; % Lower reservoir area [m2]
    Ac = 0.0738; % Cylinder cross section area [m2]
    I12 = rho*Lc/(4*Ac);
    I56 = I12;
    R23 = 2*mu*pi*Lc/Ac^2;
    R45 = R23;
    C13 = Au/(rho*g);
    C46 = Al/(rho*g);
    I = I12 + I56; % Fluid inertance [kg/m4]
    R = R23 + R45; % Fluid resistance [kg/m4s]
    C = C13*C46/(C13+C46); % Fluid capacitance [kg/m4s2]

    %Interconnection Matrix
    J_h=[0, 1/(I*C);
         -1/(I*C), 0];

    %Input Matrix
    G_h = [0;
           1/I];

    %Dissipation matrix
    R_h=[0  0;
         0  R/I^2];

    dH_h_dP_16 = C*p16 + C*rho*Lc*g;
    dH_h_dQ = I*Q;

    %Partial derivative of Hamiltonian
```

```
    dH_h=[dH_h_dP_16;
          dH_h_dQ];

    %Input
    u_h = Ps;

    %Port-Hamiltonian System Dynamics
    dx_h=(J_h-R_h)*dH_h+G_h*u_h;
end
```

```
function [E_h] = Energy_Ocean_Grazer_Hydraulic(w)

    % Parameters
    g = 9.81; % Gravitational acceleration [m/s2]
    rho = 1080; % Fluid density [kg/m3]
    mu = 0.0734; % Fluid viscosity [Ns/m2]
    Lc = 100; % Pipe length [m]
    Au = 49; % Upper reservoir area [m2]
    Al = 49; % Lower reservoir area [m2]
    Ac = 0.0738; % Cylinder cross section area [m2]
    I12 = rho*Lc/(4*Ac);
    I56 = I12;
    R23 = 2*mu*pi*Lc/Ac^2;
    R45 = R23;
    C13 = Au/(rho*g);
    C46 = Al/(rho*g);
    I = I12 + I56; % Fluid inertance [kg/m4]
    R = R23 + R45; % Fluid resistance [kg/m4s]
    C = C13*C46/(C13+C46); % Fluid capacitance [kg/m4s2]
    Lu0 = 10; % Upper reservoir initial hydraulic head [m]
    Ll0 = 30; % Lower reservoir initial hydraulic head [m]
    p10 = Lu0*rho*g;
    p60 = Ll0*rho*g;
    K = -1/2*C*(p10-p60)^2 - C*g*rho*Lc*(p10-p60);

    P_16 = w(1);
    Q    = w(2);

    Kinetic = 1/2*I*Q^2;

    Potential = 1/2*C*P_16^2 + C*g*rho*Lc*P_16 + K;

    E_h = [Potential;...
         Kinetic];

end
```

A.3 Array of point absorbers

A.3.1 Reference model

```
%% Floater blanket simulation (ODE45)
clear all; clc;
load('coef_red.mat'); % Load Ared, Cred, Fred
global Nw wi Ared Cred Floaters Amplitude Phase tr Khs kPTO dPTO m

Floaters = 10;
m = 1500; % Buoy mass [kg]
g = 9.81; % Gravitational acceleration [m/s2]
rho_sw = 1025; % Sea water density [kg/m3]
Aw = 49; % Water area 7x7
Khs = Aw*rho_sw*g; % Buoyancy coefficient [kg/s2]
kPTO = 5.8e4; % Stiffness of PTO [Nm]
dPTO = 1.1e4; % Damping of PTO [Ns/m]
Nw = 17;
wi = w(Nw); % Wave frequency [rad/s]
Amplitude = abs(Fred(Nw,:)); % Excitation force amplitude [N]
Phase = angle(Fred(Nw,:)); % Excitation force phase [rad]
tr = 80; % Ramp time [s]

% Initial conditions
initial_x = zeros(Floaters,1);
initial_dx = zeros(Floaters,1);

tspan=[0 1000];
opts = odeset('MaxStep',0.001);
[t,x]=ode45( @motion_eq, tspan, [initial_x, initial_dx], opts );
```

```
function dxdt = motion_eq(t, x)
    global Nw wi Ared Cred Floaters Amplitude Phase tr Khs kPTO dPTO m

    if t<tr
        Rf = 0.5*(1+cos(pi+pi*t/tr));
    else
        Rf = 1;
    end

    % Excitation force
    Fe = [];
    for k=1:Floaters
        Fe = [Fe; Rf*Amplitude(k)*cos(wi*t-Phase(k))];
    end

    % Radiation force
    Fr = -Cred(1:Floaters,1:Floaters,Nw)*x(Floaters+1:end);
```

```
    % Restoring force
    Fhs = -Khs*x(1:Floaters);

    % Spring-damper PTO force
    Fpto = -kPTO*x(1:Floaters) - dPTO*x(Floaters+1:end);

    % Buoy motion equation
    dx = x(Floaters+1:end);
    d2x = inv(m*eye(Floaters) + Ared(1:Floaters,1:Floaters,Nw) )*(Fe + Fhs +
        Fpto + Fr);

    dxdt=[dx; d2x];
end
```

A.3.2 Parameter identification

```
load('coef_red.mat'); load('data_param_connection.mat');

n1 = n(9,:)'; n2 = n(10,:)';
dn1 = dn(9,:)'; dn2 = dn(10,:)';
y = Fw(10,:)';


global t n1 n2 dn1 dn2 y

[p S] = fminsearch(@distance_con, [1, 1000, 1, 1000]);
```

```
function r=distance_con(params)

    lambda_alpha=params(1); k_alpha=params(2);
    lambda_beta=params(3); k_beta=params(4);

    global t n1 n2 dn1 dn2 y

    A=[-lambda_alpha 0;
        0 -lambda_beta];

    B=[k_alpha 0;
        0 k_beta];
    C=[1 1];
    D=[0 0];
    sys=ss(A,B,C,D);

    u = [n2-n1, dn2-dn1];
    [y_model,t]=lsim(sys,u,t,[0 0]);

    r = norm( y(4000001:end)-y_model(4000001:end) )

end
```

A.3.3 Model

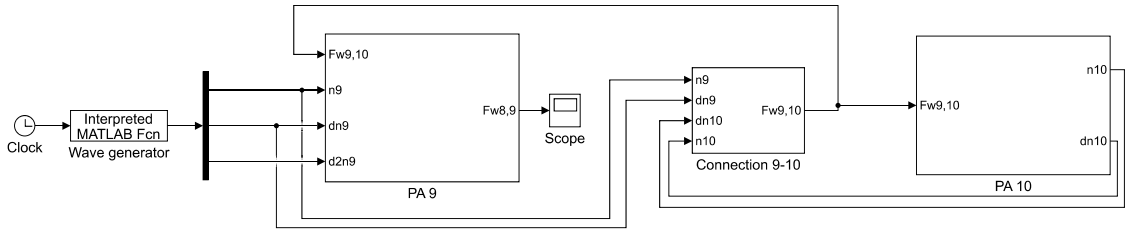

Figure A.3: Point absorbers 9 and 10 in Simulink

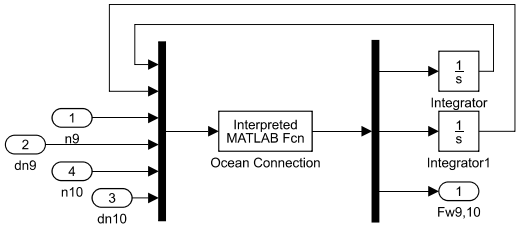

Figure A.4: Point absorbers 9 and 10 connection in Simulink

```
function y = Ocean_Connection(w)
    global lamda_alpha k_alpha lambda_beta k_beta

    alpha=w(1);
    beta=w(2);
    n1=w(3);
    dn1=w(4);
    n2=w(5);
    dn2=w(6);

    dalpha = -lamda_alpha*alpha + k_alpha*(n2-n1);
    dbeta = -lambda_beta*beta + k_beta*(dn2-dn1);
    Fw12 = alpha + beta;

    y = [dalpha, dbeta, Fw12];

end
```